



The Neuronal Circuit of the Dorsal Circadian Clock Neurons in *Drosophila melanogaster*

OPEN ACCESS

Edited by:

Ezio Rosato,
University of Leicester,
United Kingdom

Reviewed by:

Ralf Stanewsky,
University of Münster, Germany
Sheyum Syed,
University of Miami, United States

*Correspondence:

Charlotte Helfrich-Förster
charlotte.foerster@biozentrum.uni-
wuerzburg.de

*Present addresses:

Enrico Bertolini,
Center for Integrative Genomics,
Faculty of Biology and Medicine,
University of Lausanne, Lausanne,
Switzerland

Nicolas Hagedorn,
Department of Cell and Developmental
Biology, Biocentre, University of
Würzburg, Würzburg, Germany

Frank K. Schubert,
Julius Maximilian University of
Würzburg, Würzburg, Germany

†These authors have contributed
equally to this work and share first
authorship

Specialty section:

This article was submitted to
Chronobiology,
a section of the journal
Frontiers in Physiology

Received: 28 February 2022

Accepted: 28 March 2022

Published: 29 April 2022

Citation:

Reinhard N, Schubert FK, Bertolini E,
Hagedorn N, Manoli G, Sekiguchi M,
Yoshii T, Rieger D and
Helfrich-Förster C (2022) The Neuronal
Circuit of the Dorsal Circadian Clock
Neurons in *Drosophila melanogaster*.
Front. Physiol. 13:886432.
doi: 10.3389/fphys.2022.886432

Nils Reinhard^{1†}, Frank K. Schubert^{1†‡}, Enrico Bertolini^{2‡}, Nicolas Hagedorn^{1‡}, Giulia Manoli¹, Manabu Sekiguchi³, Taishi Yoshii³, Dirk Rieger¹ and Charlotte Helfrich-Förster^{1*}

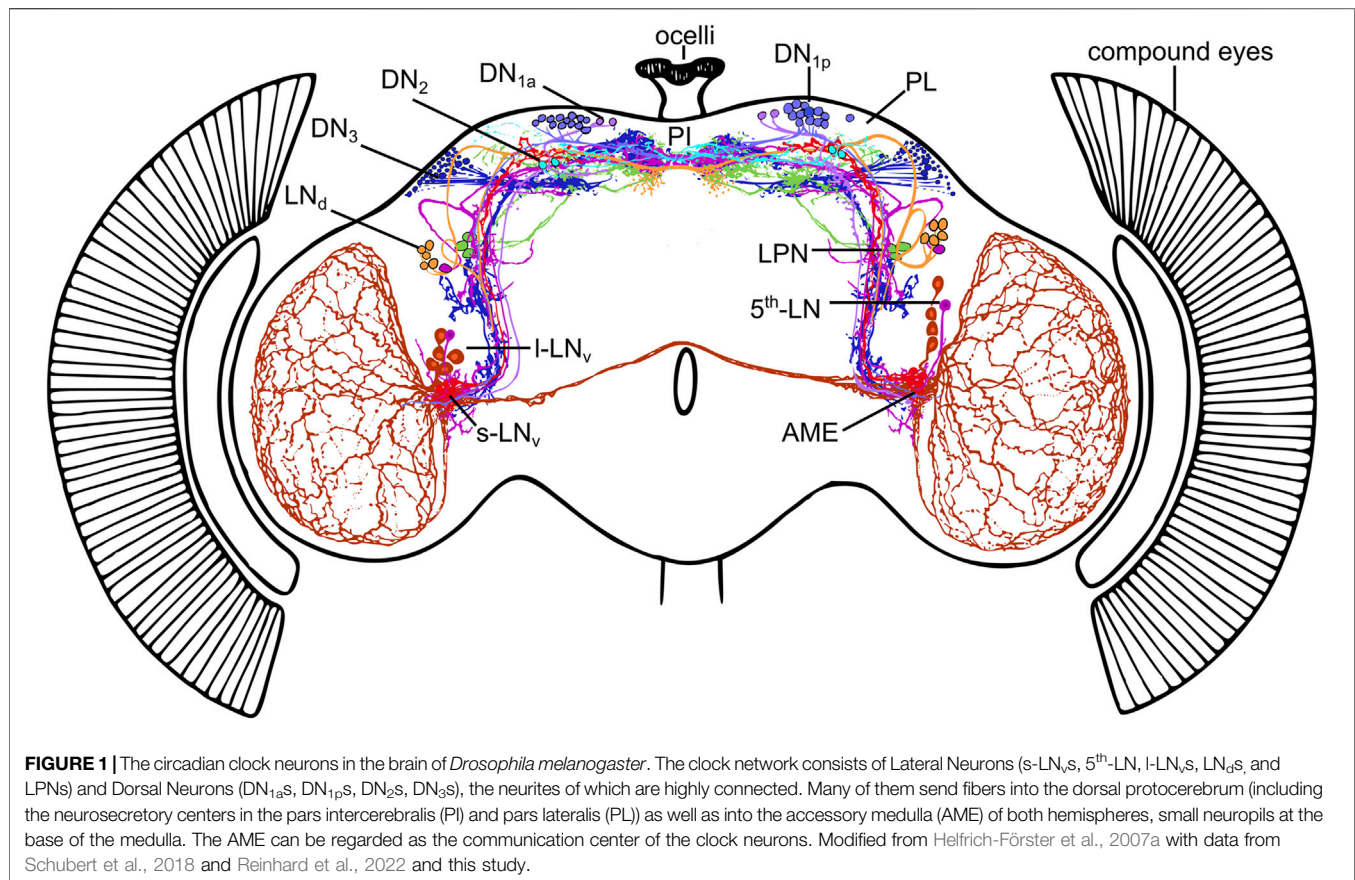
¹Julius Maximilian University of Würzburg, Würzburg, Germany, ²Neurobiology and Genetics, Theodor-Boveri-Institute, Biocenter, University of Würzburg, Würzburg, Würzburg, Germany, ³Graduate School of Natural Science and Technology, Okayama University, Okayama, Japan

Drosophila's dorsal clock neurons (DNs) consist of four clusters (DN_{1a}s, DN_{1p}s, DN₂s, and DN₃s) that largely differ in size. While the DN_{1a}s and the DN₂s encompass only two neurons, the DN_{1p}s consist of ~15 neurons, and the DN₃s comprise ~40 neurons per brain hemisphere. In comparison to the well-characterized lateral clock neurons (LNs), the neuroanatomy and function of the DNs are still not clear. Over the past decade, numerous studies have addressed their role in the fly's circadian system, leading to several sometimes divergent results. Nonetheless, these studies agreed that the DNs are important to fine-tune activity under light and temperature cycles and play essential roles in linking the output from the LNs to downstream neurons that control sleep and metabolism. Here, we used the Flybow system, specific split-GAL4 lines, *trans*-Tango, and the recently published fly connectome (called hemibrain) to describe the morphology of the DNs in greater detail, including their synaptic connections to other clock and non-clock neurons. We show that some DN groups are largely heterogenous. While certain DNs are strongly connected with the LNs, others are mainly output neurons that signal to circuits downstream of the clock. Among the latter are mushroom body neurons, central complex neurons, tubercle bulb neurons, neurosecretory cells in the pars intercerebralis, and other still unidentified partners. This heterogeneity of the DNs may explain some of the conflicting results previously found about their functionality. Most importantly, we identify two putative novel communication centers of the clock network: one fiber bundle in the superior lateral protocerebrum running toward the anterior optic tubercle and one fiber hub in the posterior lateral protocerebrum. Both are invaded by several DNs and LNs and might play an instrumental role in the clock network.

Keywords: circadian clock, *Drosophila melanogaster*, dorsal clock neurons, trans-tango, flybow, neuroanatomy, hemibrain, clock network

INTRODUCTION

Circadian clocks anticipate the 24-h rhythms on Earth. In animals, a master clock is located in the brain that tunes physiology, metabolism, and behavior to their respective temporal niche. In mammals and insects, this circadian master clock consists of tightly interacting neurons that may fulfill different roles in the clock network based on their neurochemistry, morphology and physiology (Beckwith and Ceriani, 2015; Stengl and Arendt, 2016; Helfrich-Förster, 2017; Herzog



et al., 2017; Top and Young, 2018; Rojas et al., 2019; King and Sehgal, 2020; Michel and Meijer, 2020; Mieda, 2020; Ahmad et al., 2021).

The clock network of *Drosophila melanogaster* consists of only about 150 clock neurons which can be divided according to the location of their cell bodies into five lateral and four dorsal groups. Some of them overlap with their projections in the ventrolateral brain in the so-called accessory medulla (AME) and in the dorsomedial brain, important communication centers of the clock network (**Figure 1**; Guo et al., 2016, 2018; Chatterjee et al., 2018; Fujiwara et al., 2018; Goda et al., 2018; Schubert et al., 2018; Díaz et al., 2019; Reinhard et al., 2022). So far, most attention has been focused on the lateral neurons in the anterior brain (s-LN_vs, I-LN_vs, fifth LN, and LN_ds) because some of them appear most important for driving rhythmic behavior under constant environmental conditions, in the absence of all Zeitgebers (Ewer et al., 1992; Frisch et al., 1994; Helfrich-Förster et al., 1998; Renn et al., 1999; Grima et al., 2004). More recently, the lateral neurons in the posterior brain (LPNs) have also been studied in detail and found to be involved in the control of sleep and activity patterns in the presence of light-dark or temperature cycles but not under constant environmental conditions (Chen et al., 2016; Díaz et al., 2019; Ni et al., 2019; Reinhard et al., 2022).

The four groups of dorsal neurons (DN_{1a}s, DN_{1p}s, DN₂s, and DN₃s) are the least well characterized. Like the LPNs, the DNs appear to be less important in controlling rhythmic behavior under constant environmental conditions. Nevertheless, they appear to fine-tune behavioral rhythmicity under light and temperature cycles (Miyasako et al., 2007; Picot et al., 2009; Yoshii et al., 2009; Zhang L. et al., 2010; Zhang et al., 2010 Y.; Harper et al., 2016; Chatterjee et al., 2018; Yadlapalli et al., 2018; Goda et al., 2019; Ni et al., 2019; Lamaze and Stanewsky, 2020). Furthermore, these clock neurons play essential roles in the output from the core clock network to downstream neurons. For example, they participate in the control of sleep and metabolism (Cavanaugh et al., 2014; Kunst et al., 2014; Barber et al., 2016; Guo et al., 2016, 2018; Ni et al., 2019).

Here, we used a combination of GAL4, GAL80, and newly generated split-GAL4 transgenic lines (Sekiguchi et al., 2020) to address specific groups of dorsal clock neurons that were not accessible so far. These drivers combined with the Flybow system (Hadjieconomou et al., 2011; Shimosako et al., 2014; Schubert et al., 2018) and with other tools, including *trans*-Tango (Talay et al., 2017), and electron microscopic data from the hemibrain (Scheffer et al., 2020) allowed us to characterize the anatomy and the synaptic connections of some DNs in greater detail. We will discuss our results in the light of recent physiological and

behavioral studies that provide insights into the functions of the DNs.

MATERIALS AND METHODS

Fly Strains, Husbandry, and Crossings

Unless stated otherwise, fly strains used in this study were reared on standard cornmeal medium with yeast at $25 \pm 0.2^\circ\text{C}$ and $60 \pm 5\%$ relative humidity under light-dark cycles (LD) of 12:12 h. All fly lines used are described in **Supplementary Table S1** (including references).

To reveal the anatomy of specific clock neurons, *GAL4* or split-*GAL4* lines were crossed to a membrane-bound GFP reporter (10xUAS-myr::GFP) or to a cytoplasmic myc-tagged GFP reporter (20UAS-6xGFP, **Supplementary Table S1**). They were co-stained with antibodies against the clock protein Period (PER) and different antibodies against several neuropeptides to verify their neurochemistry (see immunohistochemical procedure below). To reveal the post- and presynaptic sites of the neurons of interest, we crossed the *GAL4*-drivers to UAS-DenMark::mCherry and UAS-nSyb::EGFP, respectively (**Supplementary Table S1**).

A driver stock for usage with the Flybow system (see below) was built by balancing the *GAL4*-lines listed in Table 1 and crossing them to *y w;hs-mFlp5^{MH12}/CyO; TM2/TM6B* or to *y w;GlaBc/CyO;hs-mFlp5^{MH3}/TM6B* depending on which chromosome the *GAL4* insertion was located. Experimental flies were obtained by crossing the balanced *GAL4/hs-mFlp5* lines to either *hs-Flp¹;+;FB2.0B^{49b}* or to *hs-Flp¹;FB2.0B^{260b};+* (**Supplementary Table S1**).

Flybow

For labeling individual clock neurons we used the revised multicolor Flybow system with the *Flybow2.0B* reporter construct, which carries an FRT-site flanked stop-codon upstream of the fluorescent protein sequences (Shimosako et al., 2014). The stop codon can be removed by Flp-recombination, induced by a heat shock-promotor controlled *hs-Flp* DNA-recombinase. Experimental flies were kept at 18°C ($18 \pm 0.2^\circ\text{C}$ and $60 \pm 5\%$ relative humidity with a LD cycle of 12:12) to prevent uncontrolled Flippase recombination events. Three heat shocks (37°C) of 45–60 min were applied on three consecutive days to induce Flippase-recombinase activity at different larval and pupal stages until the clock network was fully developed, which appears to be the case in late pupal stages (Helfrich-Förster et al., 2007a). Adult flies (4–5 days after eclosion) were dissected and the brains were immunolabeled with anti-GFP, anti-mCherry, and anti-nc82 antibody-solution, as described in Schubert et al. (2018).

Trans-Tango

To reveal putative post-synaptic partners of selected clock neurons, we applied the *trans*-Tango technique (Talay et al., 2017) in combination with new clock driver lines (Sekiguchi et al., 2020). The crosses were reared at 25°C and the progeny transferred at 18°C after eclosion for several days, to obtain an

accumulation of the post-synaptic signal. In general, we sampled flies after 17, 28, 30, 34, and 53 days at 18°C and found that the post-synaptic signal strength increases significantly with time. Presynaptic neurons were revealed by anti-GFP and postsynaptic neurons by anti-Hemagglutinin (HA) antibody staining (see below and **Supplementary Table S2**).

Immunocytochemistry

Fluorescent immunocytochemistry was performed according to the protocol described in Schubert et al. (2018). In brief, male flies were fixed as whole animals for 2–3 h in 4% paraformaldehyde after they have been entrained to LD12:12 cycles for 4–5 days after eclosion. For anti-PER staining, fixation was performed 1 h before lights-on (ZT23), since PER accumulation is maximal at this time (Zerr et al., 1990). For the other antibody staining, flies were fixed around ZT3. For staining against Cryptochrome (CRY), the flies were kept several days under constant darkness to allow CRY to accumulate. After dissecting the brains in phosphate-buffered saline (pH 7.4) they were incubated in 5% normal goat serum in PBT 0.5% overnight and then incubated in the primary antibody solution for ~2 days. Fluorescent tagged secondary antibodies were applied for at least 3 h. All used antibodies are listed in **Supplementary Table S2**. The immunostained brains were aligned on a specimen slide, embedded in Vectashield 1000 mounting medium (Vector Laboratories, Burlingame, CA, United States), and stored at 4°C until scanning. If not otherwise stated at least 10 different brains were stained for each antibody or antibody combination.

Confocal Microscopy and Image Processing

Fluorescence protein expression and antibody staining were visualized and scanned with a Leica TCS SP8 or a Leica SPE confocal microscope (Leica Microsystems, Wetzlar, Germany), Leica SP8 was equipped with hybrid detectors, a photon multiplier tube, and a white light laser for excitation, using the laser and detector settings as described in Shimosako et al. (2014). Leica SPE was equipped with a photomultiplier tube and 488, 532, and 635 nm solid-state lasers for excitation.

We used a 20-fold glycerol immersion objective (HC PL APO, Leica Microsystems, Wetzlar Germany) for whole-mount scans and obtained confocal stacks with $2 \mu\text{m}$ z-step size and 1024×1024 pixels. For a more detailed view, we used a 63-fold glycerol objective (HC PL APO, Leica Microsystems, Wetzlar Germany) and scanned the brains with a resolution of 2048×2048 pixels and a z-resolution of $1 \mu\text{m}$. All focal planes were scanned three to four times and the frames were averaged to reduce background noise. The hybrid detectors of SP8 were used with photon counting mode and each focal plane was scanned and accumulated four times. The obtained confocal stacks were maximum projected and analyzed with Fiji ImageJ (Schindelin et al., 2012). Besides contrast and brightness, no further manipulations were done to the confocal images. For displaying the depth information in maximum projections we used the plug-in “Z-stack Depth Color Code” (v.0.0.2) for Fiji.

For the reconstruction of the DN_{2s}, we used the simple neurite tracer plug-in (Arshadi et al., 2021). The reconstructions were visualized using the natverse libraries (v 0.2.4, Bates et al., 2020) for RStudio (v 1.3.1093). The anti-nc82 staining (anti-bruchpilot) was used to align our stacks to the Janelia Farm Research Campus standard brain (JFRC2) by using the computational morphometry tool kit graphical user interface plug-In for Fiji (CMTK GUI, Rohlfing and Maurer, 2003; Jefferis et al., 2007). We compared our anatomical results with the results gained in the hemibrain of a single female fly (Scheffer et al., 2020) and the reconstructions of the DN_{1a}s by Marin et al. (2020) available for the full adult female brain (FAFB, Zheng et al., 2018).

Comparison With Electron Microscopic Reconstruction Data

For a comparison of our findings with the reconstructed neurons of the electron microscopic data set from the hemibrain and the FAFB, we used the natverse libraries (v 0.2.4, Bates et al., 2020) and hemibrainr package (v.0.5.0, Bates and Jefferis, 2022) for R (v. 4.0.5) via RStudio (v 1.3.1093). The neuron-specific information was obtained from the hemibrain dataset (Scheffer et al., 2020, v 1.2.1) of the neuprint server (neuprint.janelia.org). For the FAFB dataset (Zheng et al., 2018) the reconstructions were obtained from the Virtual Fly Brain CATMAID server (fafb.catmaid.virtualflybrain.org). The annotation of the neurons was used as a reference and the identity of the neurons was verified by their morphology and the orientation in the brain if possible. For morphological comparisons, the neurons and brain regions of the hemibrain were transformed into the JRC 2018F template space (Bogovic et al., 2020) using xform_brain (nat.templatebrains v 1.0). When different neuron types were shown in the same brain, the neurons were additionally mirrored to the other hemisphere. Connectivity data was visualized using the ggplot2 package (v3.3.5, Wickham, 2016).

RESULTS

To facilitate understanding, we describe the morphology and synaptic connectivity of the different dorsal neurons in the context of the existing literature and, where appropriate, discuss the reasons for differences between studies.

The DN_{1a}s

The DN_{1a}s express PER from the first larval instar onward (Kaneko et al., 1997). They are glutamatergic (Hamasaoka et al., 2007; Collins et al., 2012) and in adult flies, they express additionally the neuropeptides IPNamide (Shafer et al., 2006) and CChamide1 (Fujiwara et al., 2018). Furthermore, they express the intracellular blue-light receptor Cryptochrome (CRY) (Yoshii et al., 2008). We addressed the two DN_{1a}s with Flybow using the *R16C05-GAL4* driver (Pfeiffer et al., 2008). Using this method, we were able to trace individual DN_{1a}s in 30

brains, whereas in 11 brains only a single DN_{1a} was labeled and could be analyzed at the single-cell level. In addition, the two DN_{1a}s were stained together in the DN_{1a}-specific split-GAL4 line *R43D05-p65.AD; R93B11-DBD* (Sekiguchi et al., 2020). In the following, we will describe the morphology of the DN_{1a}s according to the results of both staining methods compared to the reconstructions at the electron microscopic level (**Supplementary Video S1**).

The cell bodies of both DN_{1a}s are located in the anterior superior cell body rind dorsal to the superior lateral protocerebrum (SLP) (Shafer et al., 2006). Initially, the DN_{1a}s project ventrally along the surface of the SLP into the posterior-most part of the SLP. The projections of both cells bifurcate at the level of the posterior boundary between the lateral horn (LH) and the SLP and invade the posterior-most part of the LH. Here, the neurites of both DN_{1a}s branch extensively and innervate the ventromedial region of the posterior LH (**Figure 2C**), together with the s-LN_v terminals. Both neurons send projections medially that terminate dorsally to the Kenyon cells of the mushroom bodies in the lateral and dorsal accessory calyx (CA, **Figures 2A,C**, arrow). Further projections run ventrally to the accessory medulla (AME, **Figure 2**, open arrowhead). Concerning the shape and extent of arborizations in the posterior SLP and LH, the two neurons differed slightly. The varicose arborizations of one DN_{1a} appeared slightly more restricted around the CA whereas the other DN_{1a} showed less dense projections, extending slightly more medially in the SLP as well as more ventrally in the posterior LH. The biggest difference between the two DN_{1a}s represented the single neurite of the neuron with the slightly broader arborization pattern, reaching from the dense ramifications around the CA in the dorsal SLP (**Figure 2** double arrowhead). In roughly one-third of the DN_{1a}s analyzed with Flybow the projections to the AME were not visible. However, the DN_{1a}-specific split-GAL4 line revealed that both DN_{1a}s project ventrally (**Figure 2C** open arrowhead). This projection ran parallel to the neurites of the Pigment Dispersing Factor (PDF)-positive s-LN_vs until it reached and joined the posterior optic commissure (**Figures 2A,C**, open arrow). Along with this major fiber bundle, the ventral DN_{1a} projections invaded the ipsilateral AME and often ran onto the surface or along the anteromedial edge of the medulla (**Figures 2A,C**). Due to the vast overlap of their arborizations in most parts, distinguishing the two neurons in the polarity staining was difficult. We observed signals of the post- and presynaptic markers in the posterior ventromedial LH, probably originating from both DN_{1a}s. The presynaptic vesicles in the projection to the AME were consistently and strongly labeled (nSyb::EGFP), whereas only a faint DenMark (TLN::mCherry) signal (postsynaptic marker) was found in these neurites (**Figures 2D,E**).

The reconstructions of the hemibrain largely support our observations and the two annotated DN_{1a}s (#264083994 and #5813022274) have the same characteristic arborization pattern as described above (**Figure 2F**). The reconstructions by Marin et al. (2020) using the FAFB dataset (**Figure 2F**, neuron #4129363 and #3973434) support additionally our observation that the DN_{1a}s differ in the neurite reaching in the dorsal SLP

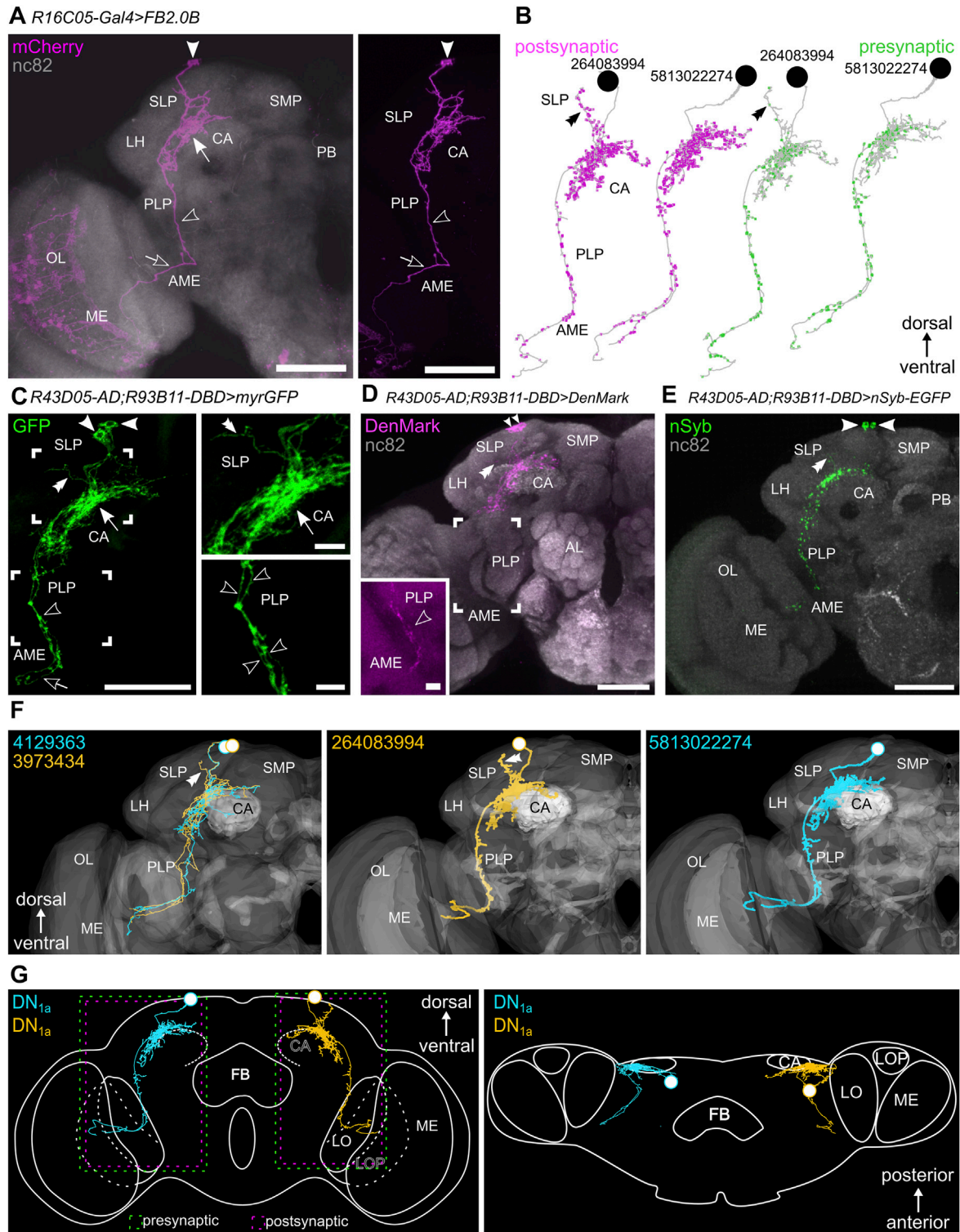


FIGURE 2 | The morphology of the two DN_{1a} s. **(A)** Flybow-reporter expression (mCherry, magenta) driven by *R16C05-GAL4* and anti-nc82 neuropil staining (gray). Only one of the two DN_{1a} s is labeled together with several small cells in the optic lobe. A single fiber of this neuron projects from the SLP through the ventromedial lateral horn (LH) and the posterior lateral protocerebrum (PLP) into the accessory medulla (AME) and further toward the surface of the medulla (ME) (open arrow). The arrow points to its dense arborizations around the mushroom body calyx (CA). **(B)** Postsynaptic (magenta) and presynaptic (green) sites of the two DN_{1a} s (revealed in the hemibrain) are distributed over the entire neurons. **(C)** Morphology of both DN_{1a} s visualized in the highly DN_{1a} specific split-GAL4 line with membrane-bound GFP (maximal projection of 47 confocal planes). Both DN_{1a} s project to the AME (open arrow and arrowhead) and only differ by a faint anteriorly projecting fiber in the SLP (arrowhead). **(D)** Morphology of the neuron 264083994 visualized in the highly DN_{1a} specific split-GAL4 line with membrane-bound DenMark (magenta) and anti-nc82 neuropil staining (gray). **(E)** Morphology of the neuron 5813022274 visualized in the highly DN_{1a} specific split-GAL4 line with membrane-bound nSyb (green) and anti-nc82 neuropil staining (gray). **(F)** Maximal projections of the three neurons in gray. The neuron 264083994 is highlighted in yellow and the neuron 5813022274 in cyan. **(G)** Schematic diagrams of the neurons in dorsal/ventral and posterior/anterior views. Presynaptic sites are shown in green and postsynaptic sites in magenta. (Continued)

FIGURE 2 | (double arrowhead, see also inset). The insets show magnifications of the arborizations close to the CA and the PLP. **(D)** Staining against the DenMark reporter (mCherry) which visualizes the dendritic fibers of the DN_{1a}s. The inset shows a magnification of the ventrally running fibers towards the AME with a maximal projection of only 15 confocal planes for clarification. **(E)** GFP staining of the nSyb-EGFP fusion protein that visualizes the axonal terminals of the DN_{1a}s. **(F)** Reconstructions of the two DN_{1a}s on the electron microscopic level derived from the FAFB (Marin et al., 2020) and the hemibrain (Scheffer et al., 2020). The double arrowhead highlights the anterior running arm of one of the two DN_{1a}s (yellow). **(G)** Schematic overview of the DN_{1a} morphology from a frontal (left) and dorsal (right) view. The rectangles with dashed lines in the left picture represent post- and presynaptic sites as revealed by DenMark and nSyb staining, respectively. LOP, lobula plate; LO, lobula; CA, mushroom body calyx; SLP, superior lateral protocerebrum; SMP, superior medial protocerebrum; LH, lateral horn; AL, antennal lobes; PB, protocerebral bridge; OL, optic lobes; FB, fan-shaped body; ME, medulla; Scale bars represent 50 and 10 μm in detail views.

(**Figure 2F** double arrowhead). Output synapses (presynaptic terminals) were present throughout the neurites, but less densely in the one fiber of DN_{1a} #264083994 that projects dorsally into the SLP. This dorsally projecting fiber carried mainly input synapses (postsynaptic terminals) (**Figure 2B** double arrowhead).

Synaptic Partners of the DN_{1a}s

Both DN_{1a}s appear strongly linked to the s-LN_vs. The neurites of both neuron types have been shown to largely overlap with each other (Fujiwara et al., 2018), an observation that we confirm with our study. The DN_{1a}s overlap with the terminals of the s-LN_vs in the SLP and with the dendrites of the s-LN_vs in the AME. Also functionally, the DN_{1a}s and the s-LN_vs are connected as was shown by previous work: the DN_{1a}s signal *via* glutamate and the neuropeptide CCHamide1 to the s-LN_vs (Hamasaka et al., 2007; Collins et al., 2012; Fujiwara et al., 2018; Song et al., 2021) while the s-LN_vs signal *via* glycine and PDF to the DN_{1a}s (Shafer et al., 2008; Yoshii et al., 2009; Frenkel et al., 2017). To further investigate this mutual synaptic connection and to identify synaptic outputs of the DN_{1a}s to other downstream neurons we performed *trans*-Tango and visualized the results by anti-HA in flies of different ages (17, 28, 30 days).

When driving *trans*-Tango in the DN_{1a}s, several clock neurons (PER-positive) were co-labeled by the HA-antibody (**Figures 3A,B**): one to two DN₃s, the Ion transport peptide (ITP)-positive LN_d and fifth LN, one to four s-LN_vs (**Figures 3A,B**, white arrows) and sometimes weakly one to four l-LN_s as already shown by Song et al. (2021). Also, the DN_{1a}s themselves were labeled in some brains. In addition, one characteristic neuron of the dorsal fan-shaped body (dFB) was marked by anti-HA. Its cell body was located in the posterior brain (**Figure 3A** magenta arrowheads) with neurites running into the eighth layer of the FB and laterally toward a dense fiber hub close to the LPNs, in which several clock neurons arborize and the DN_{1a}s contribute few fibers (**Figure 3A**, magenta arrows; *see also later*). Further non-clock neurons were labeled in the lateral, dorsolateral and posterior dorsal brain. These were located close to the LN_ds, DN₃s, and DN_{1p}s, respectively, but were not double-labeled by anti-PER (**Figures 3A,B**, open magenta arrowheads). While the DN₃s and most of the LNs were already stained in young flies, the neuron projecting to the dFB was only marked in older flies.

When driving *trans*-Tango in the s-LN_vs, we found that at least one DN_{1a} is postsynaptic to the s-LN_vs (**Figure 3C**). In addition, the three CRY-negative LN_ds were marked, indicating that they are also postsynaptic to the s-LN_vs.

The *trans*-Tango staining was rather consistent with the presynaptic (output) sites of the DN_{1a}s revealed on the ultrastructural level in the hemibrain (**Figure 4A**). Most

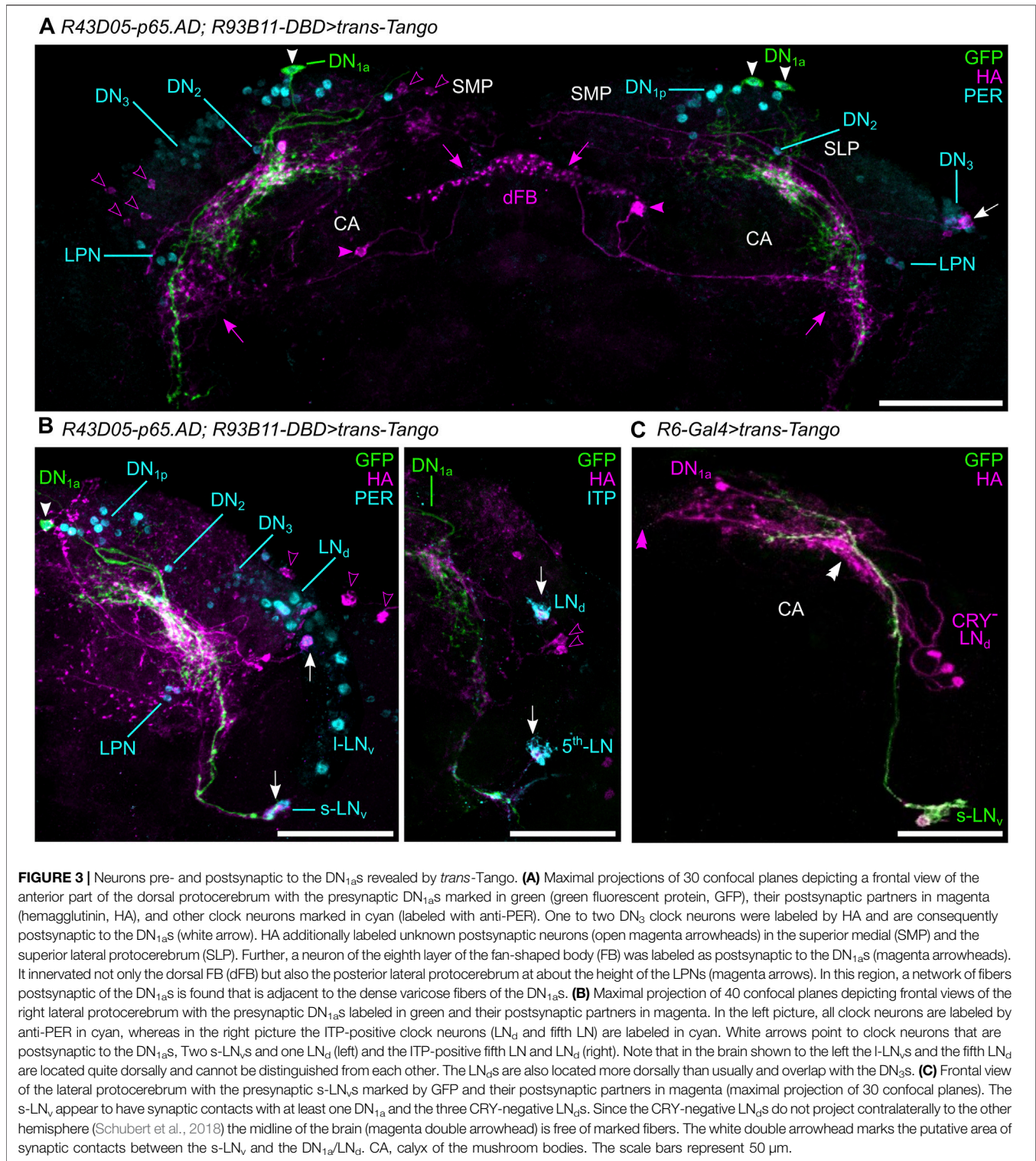
output synapses were found in the superior protocerebrum (SLP and SMP) to the ITP- and CRY-positive LN_d and the fifth LN, but no outputs were found to the s-LN_vs (**Figure 4A**) and very few to DN₃-like neurons (*see below*). The virtual lack of output to the DN₃s is understandable because these neurons are not unequivocally annotated in the hemibrain, but it is less clear why the s-LN_vs are not among the listed postsynaptic partners of the DN_{1a}s. Most probably, they form only a small amount of synapses with these clock cells that have been overlooked. The same might be true for the input synapses from the s-LN_vs that we detected in our *trans*-Tango staining. The s-LN_vs are not listed as input partners of the DN_{1a}s in the hemibrain (**Figure 4B**). Nevertheless, input from the s-LN_vs to the DN_{1a}s was also revealed in a recent functional study, strongly indicating that our observation is valid (Song et al., 2021).

As expected from the slightly different morphology of the two DN_{1a}s, DN_{1a} #264083994 with the predominantly dendritic fiber in the SLP received slightly more input from neurons located in this brain region. Otherwise, the two DN_{1a}s show large similarities in their synaptic connections (**Figure 4C**) and seem to signal to each other (**Figure 4B**).

While the main DN_{1a} input and output synapses are formed in the SLP and posterior lateral protocerebrum (PLP), their neurites in the AME appear mainly presynaptic. The DN_{1a}s get especially strong input (20% of their input synapses) in the dorsal and lateral accessory calyxes that are located adjacent to the SLP (**Figure 4C**). Most of this input appears to come from temperature sensing neurons in the antennal lobes (VP3+_vPN/VP2+_adPN as well as VP2_adPN, **Figure 4B**) as was also revealed by Marin et al. (2020).

The DN_{1p}s

The DN_{1p}s are a demonstrably heterogeneous group in respect to their neurochemistry and morphology. About half of the approximately 15 cells per brain hemisphere express CRY and the PDF receptor (PDFR) (Shafer et al., 2008; Yoshii et al., 2008; Im and Taghert, 2010). Five to six of the CRY-positive DN_{1p}s are positive for glutamate (Hamasaka et al., 2007; Guo et al., 2016) and the Diuretic Hormone 31 (DH31, Kunst et al., 2014; Goda et al., 2016) and at least four of these CRY-/DH31-positive neurons express additionally Allatostatin C (AstC, Díaz et al., 2019; Zhang et al., 2021) and CNMamide (Jung et al., 2014; Abruzzi et al., 2017; Jin et al., 2021; Zhang et al., 2021). As recently shown, four AstC-positive DN_{1p}s additionally express the receptors for PDF and DH31 (Goda et al., 2018; Lin et al., 2022). The neurochemistry of the CRY-/PDFR-negative DN_{1p}s is so far unknown.



It is not surprising that the DN_{1p}s differ also in their morphology. The latter has been described in detail in three studies coming from different labs (Chatterjee et al., 2018; Guo et al., 2018; Lamaze et al., 2018). These studies used combinations of different *GAL4*, *LexA*, *GAL80*, and split-*GAL4* lines to address

different subgroups of the DN_{1p}s and stochastic flip outs to label single neurons. The most important line, which we used also in our study, is the *Clk4.1M-GAL4* line. It targets about 10 out of the 15 DN_{1p}s comprising the majority (~6 out of 7) of the CRY-positive neurons plus ~4 CRY-negative cells (Figure 2; Zhang Y.

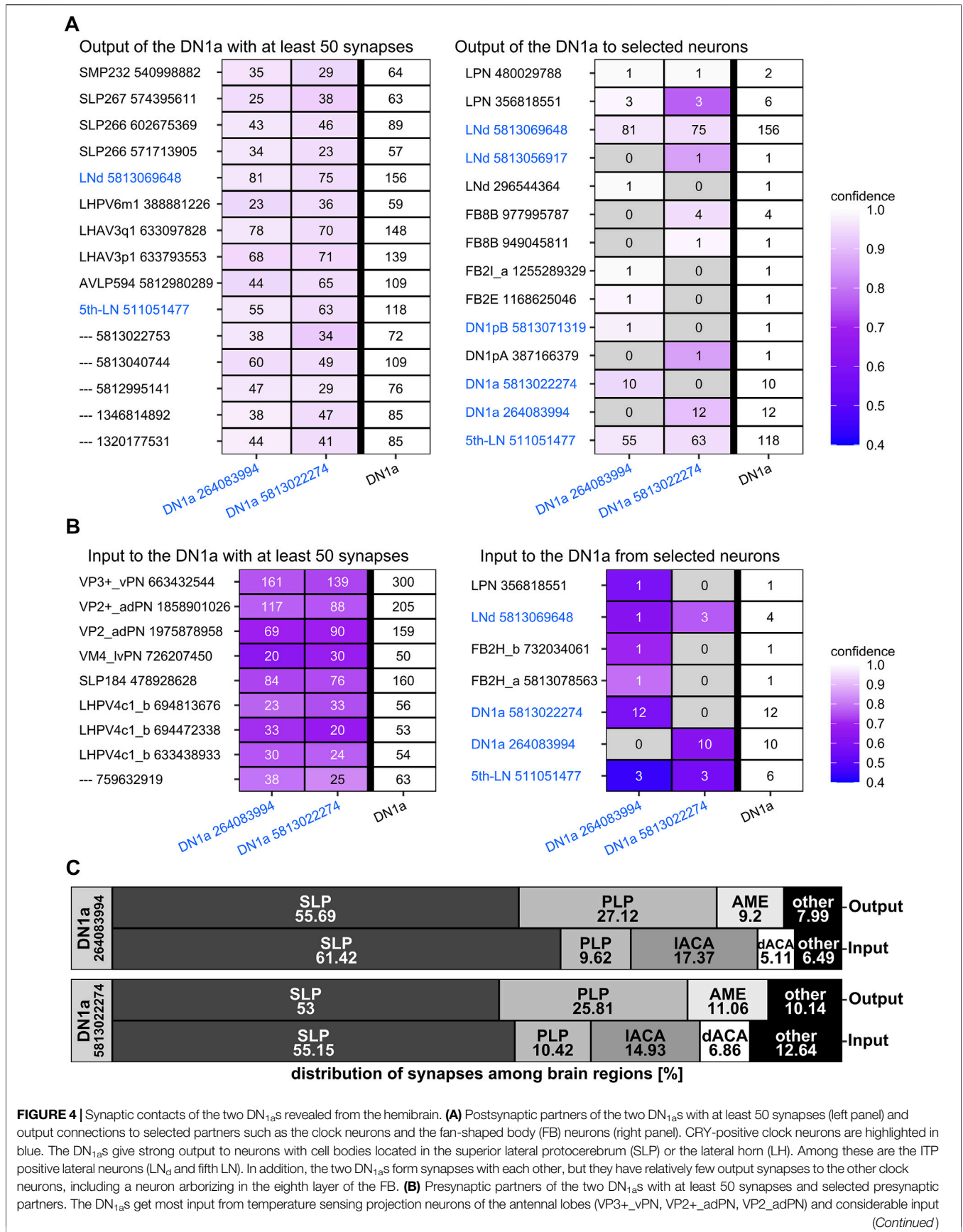


FIGURE 4 | from neurons with cell bodies in the LH and SLP. Only little input comes from the clock neurons. **(C)** Synapse distribution of the two DN_{1a}s among the brain regions. The DN_{1a}s form about 50% of their input and output synapses in the SLP. In the second place are output synapses in the PLP, an area from which they also get input, although to a lower amount. Furthermore, they give output to the AME but do not receive input worth mentioning from there. Instead, they receive considerable input from the lateral and dorsal accessory calyx (LACA, dACA). As can be expected from their similar morphology, the two DN_{1a}s largely coincide in synapse distribution and synaptic partners.

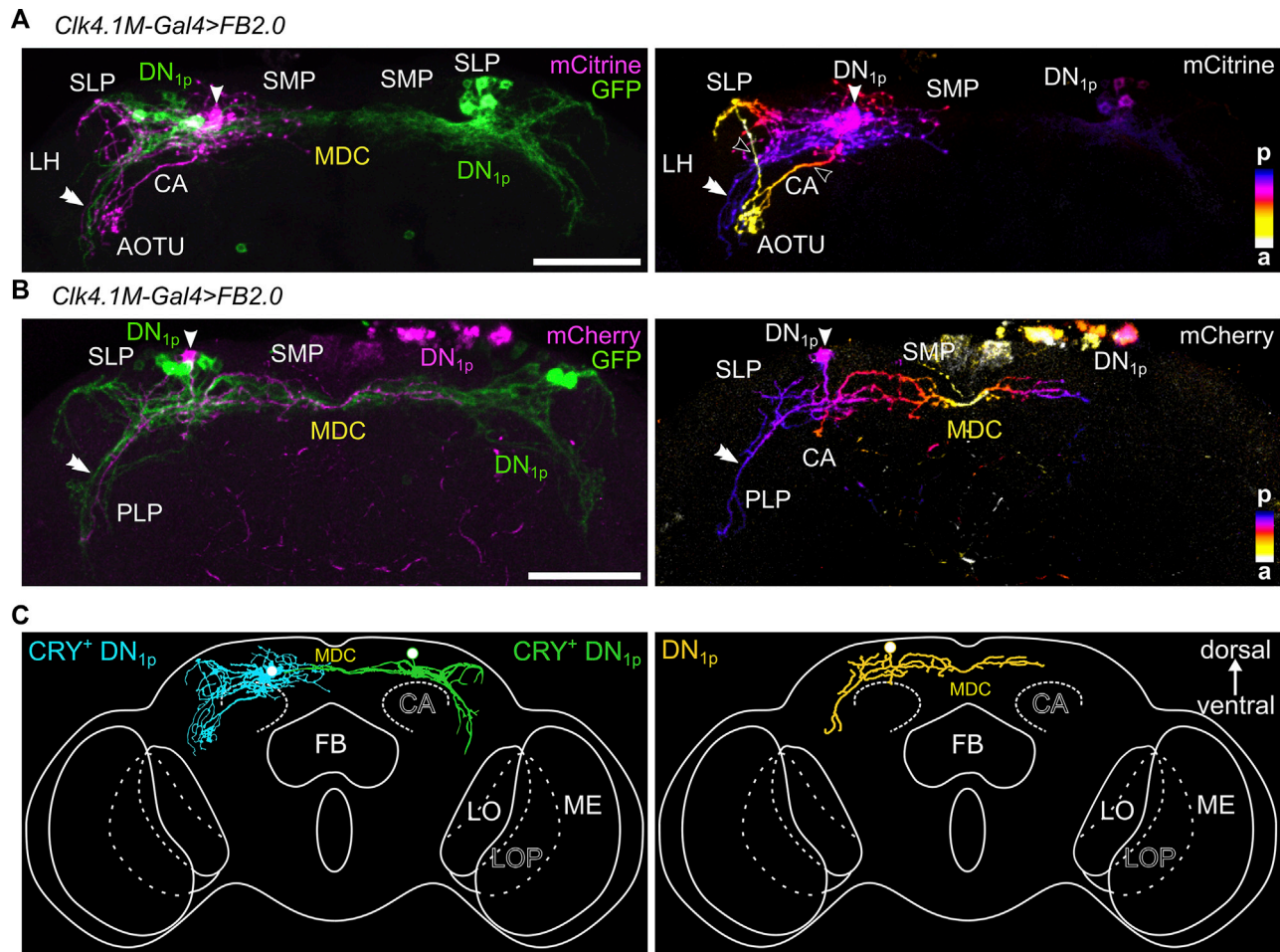


FIGURE 5 | Different morphological subtypes within the DN_{1p}s as revealed by Flybow staining. **(A, B)** *Clk4.1M-GAL4* driven Flybow-reporter expression in different DN_{1p}s. The left panels show the original Flybow-reporter expression in which an individually labeled neuron (magenta, arrowhead) expresses mCitrine or mCherry, while several other DN_{1p}s express the default GFP reporter (green). The right panels depict the single DN_{1p}s that are marked in magenta in the left panels with color-coded depth information (anterior (a) in yellow colors, posterior (p) in blue colors as shown in the color code bars in the right bottom of each figure). **(A)** mCitrine marks a single neuron with arborizations in the superior lateral protocerebrum (SLP). Two fibers (open arrowheads) run anterior to the lateral anterior optic tubercle (AOTU), where they arborize prominently. Another fiber (double arrowhead) remains in the posterior brain and runs ventrally following the s-LN_v projections. **(B)** Single DN_{1p} expressing mCherry (magenta) among four other GFP expressing DN_{1p}s. The single DN_{1p} has a prominent fiber following the path of the s-LN_vs in the ipsilateral posterior lateral protocerebrum (PLP) and crosses the dorsoventral midline of the brain through the middle dorsal commissure (MDC). No arborizations in the anterior SLP are visible. **(C)** Schematic depiction of the three DN_{1p} subtypes identified by Flybow. SMP, superior medial protocerebrum; LH, lateral horn; PLP, posterior lateral protocerebrum; ME, medulla; LO, lobula; LOP, lobula plate; FB, fan-shaped body. Scale bars represent 50 μ m.

et al., 2010; Zhang et al., 2010 L; Chatterjee et al., 2018). The *R18H11-GAL4* line from the FlyLight library collection (Pfeiffer et al., 2008) originates from the gene coding for PDFR and targets only the five to six CRY-/PDFR-positive neurons that are additionally glutamate- and DH31-positive (Kunst et al., 2014; Goda et al., 2016; Guo et al., 2016, 2018; Chatterjee et al., 2018). In

contrast, the *R18H11-LexA* line additionally drives in few CRY-/PDFR-negative DN_{1p}s (Chatterjee et al., 2018; Guo et al., 2018), presumably because PDFR expression is not completely absent in the PDFR-negative characterized neurons, but only largely reduced, so that it is still revealed by strong drivers. Nevertheless, none of the used lines targets all DN_{1p}s, so

additional types of DN_{1p}s may exist (especially CRY-negative ones) that have not yet been characterized.

Previous studies have principally identified two main types of DN_{1p}s: One type remaining ipsilaterally and projecting to the anterior optic tubercle (AOTU) (the so-called anterior projecting dorsal neurons), while the other type crosses the midline of the brain through the pars intercerebralis but lacks projections to the AOTU (Chatterjee et al., 2018; Lamaze et al., 2018). According to Chatterjee et al. (2018), the DN_{1p}s projecting to the AOTU express CRY, whereas it is unclear which DN_{1p}s of the other type are CRY-positive.

We analyzed the DN_{1p}s of 22 *Clk4.1M-GAL4* brains in combination with the Flybow-reporter to reveal potential differences in the morphology of the DN_{1p}s. As it turned out, the modified Flp-recombinase had not been activated sufficiently, and only four brains showed individually labeled neurons. Nevertheless, we were able to identify three different types of DN_{1p} subgroups. All DN_{1p} cell bodies were located in the dorsal posterior cell body ring innervating the posterior superior medial protocerebrum (SMP) and SLP, as well as the posterior ventromedial LH and dorsal parts of the PLP, where they followed the s-LN_v projections in ventral direction, although no fibers reached the AME (Figure 5).

A single labeled DN_{1p} largely resembled the previously described CRY-positive neurons that invade the AOTU and form pronounced varicosities in this region (Figure 5A, called a-DN_{1p} in Lamaze et al., 2018). The fibers of this neuron formed two loops running from posterior to anterior and terminated in the AOTU (open arrowheads). One loop ran around the SLP and the second one ventrally on the surface of the superior clamp (SCL) and the inferior clamp until both converged shortly before the AOTU. In addition, fibers from this neuron remained posterior and followed the s-LN_v projections in the PLP (double arrowhead) for a short distance toward the AME. Most significantly, all neurites of this neuron remained ipsilaterally and did not cross the midline of the brain in the middle dorsal commissure (MDC). A similar neuron is described in Figures 1C,D of Lamaze et al. (2018) and called anteriorly projecting DN_{1p} (a-DN_{1p}).

The other labeled DN_{1p}s appeared to belong to the second type of DN_{1p}s described by Lamaze et al. (2018), Chatterjee et al. (2018), and Guo et al. (2018). These neurons were called vc-DN_{1p}-neurons by Lamaze et al. (2018) and sent fibers through the MDC to the contralateral SMP and on the ipsilateral side, their projections in the PLP appeared to reach slightly further toward the AME than that of the first DN_{1p} type (Figure 5B). We could identify two different subtypes with this projection pattern. One neuron of the first subtype was individually labeled (Figure 5B right and yellow neuron in Figure 5C), whereas the presence of the second subtype (Figure 5C green) was concluded from the samples with varying numbers of visible cells. Fibers of the second subtype started to form a loop around the SLP as was typical for the two CRY-positive DN_{1p}s described above, but they did not complete this loop and did not reach the AOTU (green neuron in Figure 5C). A very similar neuron (called vc-DN_{1p}) is described in Figure 1C of Lamaze et al. (2018). Furthermore, similar DN_{1p}s were found in Jin et al. (2021; Figure 5E in Jin et al.) and Zhang et al. (2021; Figure 3C in

Zhang et al.) among the CNMamide-positive neurons. Since the latter are CRY-positive, we assume that this type of DN_{1p} is CRY-positive. In case of the yellow colored neuron in Figure 5C, we do not know about its CRY expression. Therefore, no statement about CRY is made. The same applies for all further statements regarding the DN_{1p}s.

Seven DN_{1p}s are annotated in the hemibrain, which were again divided into two types (called A and B in the hemibrain) (Figures 6–8 and Supplementary Video S2). The two type B neurons (cyan in Figure 6) resemble CRY-positive neurons described above, which remain ipsilateral and project into the AOTU. The five type A neurons all project contralaterally and do not enter the AOTU (green and magenta in Figure 6). Among these, the DN_{1p} depicted in green closely resembles the just described CRY-/CNMamide-positive DN_{1p}s that send fibers into the anterior SLP and follow the s-LN_v projections in the PLP several micrometers (green in Figure 6). The other four type A neurons do not show any fibers following the s-LN_v projections in the PLP, while the fibers extending toward the anterior SLP were generally present (magenta in Figure 6). The DN_{1p} neuron type that is not annotated in the hemibrain is depicted in Figure 5C (yellow). This neuron completely lacks the anterior running fibers but shows prominent neurites following the s-LN_v projections in the PLP. A similar neuron is described by Lamaze et al. (2018; vc-DN_{1p} neuron in Figure 1D) making us confident that this is a true subtype.

Synapses and Putative Synaptic Partners of the DN_{1p}s

Previous studies used diverse GAL4 lines to perform syt-GFP (Guo et al., 2016, 2018; Lamaze et al., 2018) and DenMark staining (Chatterjee et al., 2018; Guo et al., 2018; Lamaze et al., 2018) and revealed putative presynaptic output sites of the DN_{1p}s in the SMP close to the pars intercerebralis and in the AOTU, to which the CRY-positive DN_{1p}s project (Guo et al., 2018; Lamaze et al., 2018). Chatterjee et al. (2018) found that the characteristic anterior projecting loops of the CRY-positive DN_{1p}s around the SLP are not only presynaptic but also dendritic.

We used the connectome data of the hemibrain (Scheffer et al., 2020) to reveal the input and output sites of the DN_{1p}s and could confirm the results of Chatterjee et al. (2018) and specify the results of the other studies. While the input and output sites of the CRY-positive DN_{1p}s (type B neurons) are equally distributed across the entire surface of the neurons, the type A DN_{1p}s show output sites mainly in the SMP, while they receive input along the whole neuron (Figures 6E–G, Figure 8, Figure 9). This is true for all type A neurons independent of the subtype (Figure 8).

Trans-Tango staining by Guo et al. (2018) revealed some LN_ds and tubercle bulb neurons as possible postsynaptic partners of the DN_{1p}s, as well as weak signals in some DN_{3s}. Here, we used again the connectivity data from the hemibrain (Scheffer et al., 2020) to investigate the pre- and postsynaptic partners of the DN_{1p}s in more detail. Since we found a strong difference between the CRY-positive type B and the more heterogeneous type A DN_{1p}s, we analyzed the two groups separately (Figures 7–9). The type A DN_{1p}s show mainly output to CRY-positive clock neurons with the strongest synaptic output to the ITP and CRY-positive LN_d and fifth LN (Figure 7A). Other clock neurons are only contacted

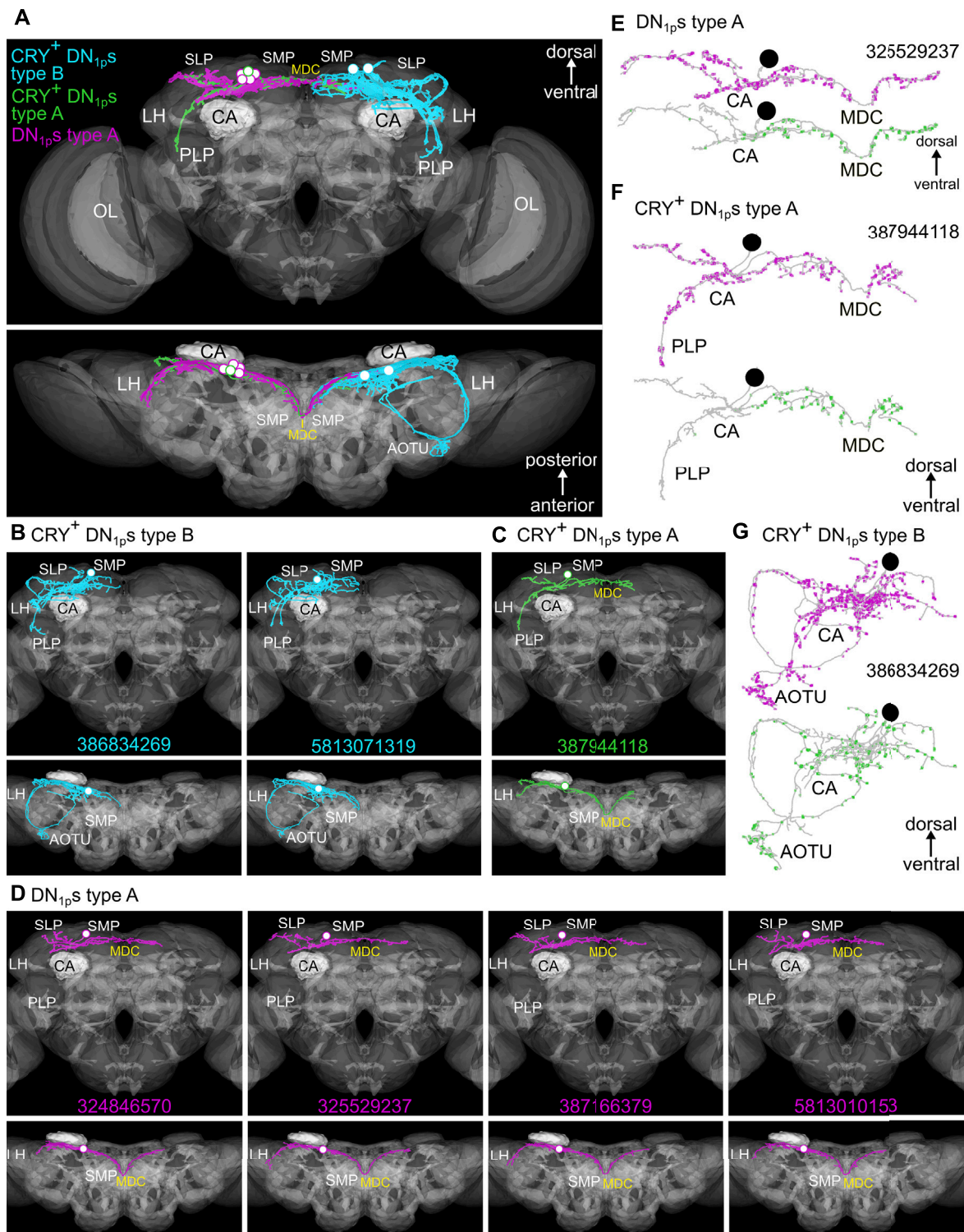


FIGURE 6 | The different morphologies of the seven DN_{1p}s annotated in the hemibrain. **(A)** Standard brain (JRC 2018F) showing the three different morphological subtypes among the seven DN_{1p}s annotated in the hemibrain. The presumably CRY-positive neurons are depicted in cyan and green, while the still undefined DN_{1p}s are shown in magenta. **(B)** Detailed representation of the two Type B CRY-positive DN_{1p}s in ventral-dorsal (top) and anterior-posterior (bottom) orientation. Both neurons arborize in the superior lateral protocerebrum (SLP), the superior medial protocerebrum (SMP), and project ventrally to the posterior lateral protocerebrum (PLP). Additionally, they send two fibers to the anterior optic tubercle (AOTU) each of them forming a loop that runs on the dorsal and ventral surface of the SLP, respectively (compare with **G**). **(C)** Representation of the type A CRY-positive DN_{1p} (#387944118). The projections of this neuron remain mostly posterior. In the SLP, this DN_{1p} also (Continued)

FIGURE 6 | sends one fiber toward the AOTU but does not reach it. In further contrast to the two Type B CRY-positive DN_{1p}s neurons, it projects via the middle dorsal commissure (MDC) to the contralateral superior medial protocerebrum (SMP). **(D)** Representation of four type A DN_{1p}s with still undefined nature. These neurons are morphologically similar to the type A CRY-positive DN_{1p} and cross the midline in the MDC, but they remain completely in the SLP and SMP and do not send fibers to the PLP. **(E–G)** postsynaptic (input, magenta) and presynaptic (output, green) sites of the three different DN_{1p} subtypes. **(E,F)** Type A DN_{1p}s receive input all over their neurites but restrict output to the ipsilateral and contralateral SMP. **(G)** Type B DN_{1p}s receive input and give output all over their neurites. CA, mushroom body calyx; LH, lateral horn; OL, optic lobes.

with very few synapses and likewise the output to non-clock neurons is generally weak. The connection to the ITP and CRY-positive LN_d and the fifth LN appears reciprocal since type A DN_{1p}s also receive strong input from these two neurons (**Figure 7B**). Otherwise, the type A DN_{1p}s get little input from the clock network (**Figure 7B**).

As already shown by Guo *et al.* (2018), the CRY-positive type B DN_{1p}s signal to tubercle bulb neurons as well as to tubercle-tubercle neurons which connect both AOTUs (**Figure 9A**). Additionally, we found that they signal strongly to at least one DN₂ (**Figure 9A**), whereas their synaptic contact with other clock neurons is rather weak. Their weak contact within the clock network also concerns the ITP- and CRY-positive LN_d and fifth LN, which have strong reciprocal synaptic connections with the Type A DN_{1p}s (**Figure 9A**). There is also very little synaptic input from the clock network to the CRY-positive type B DN_{1p}s (**Figure 9B**).

The DN₂s

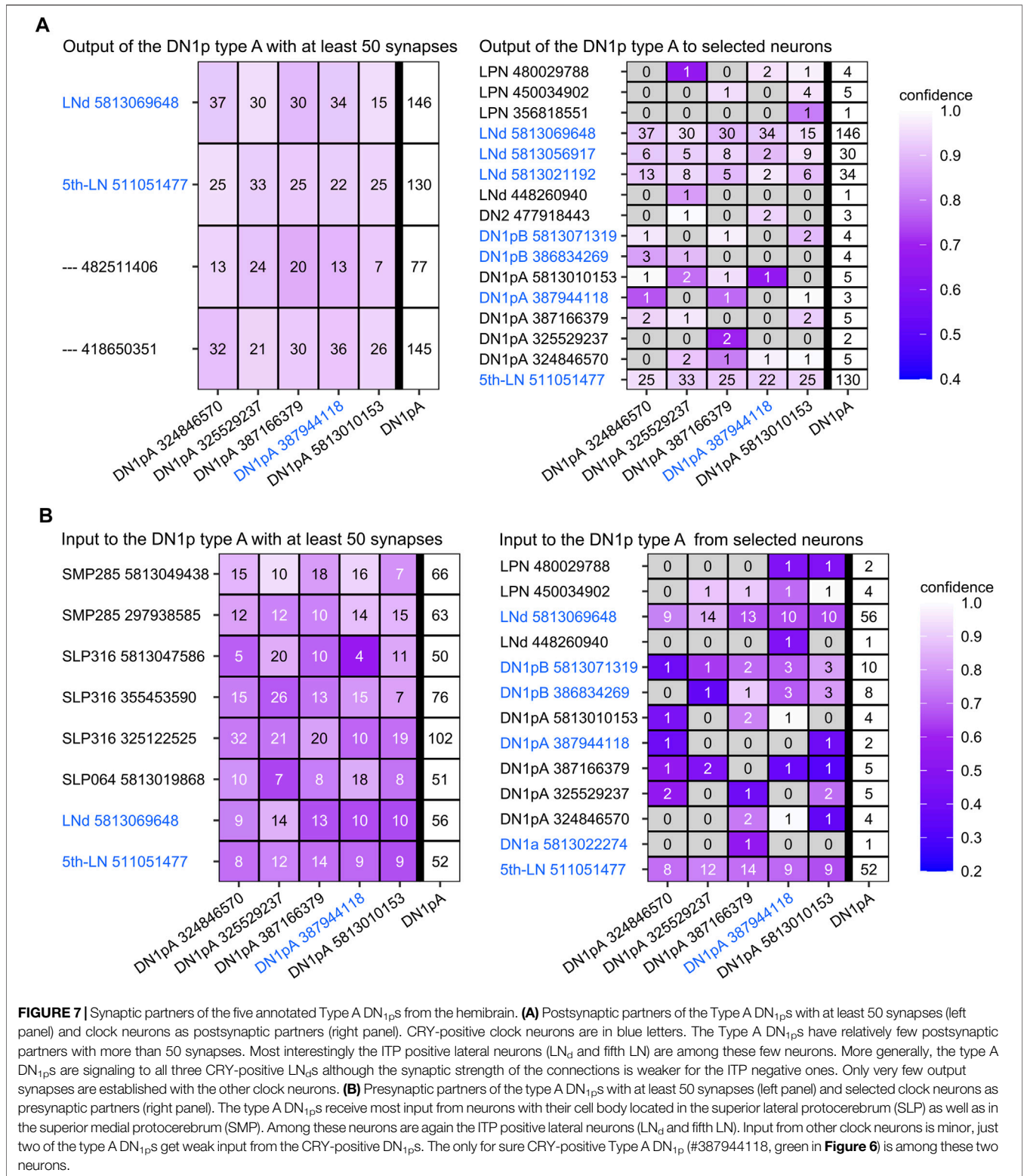
The DN₂s consist of only two neurons that have been described for the first time 25 years ago (Kaneko *et al.*, 1997). Their importance in the clock network is highlighted by their early appearance during larval development, together with the s-LN_vs, the fifth LN, and the DN_{1a}s, but their function and fine anatomy are yet unclear. The somata of the DN₂s are located near the dorsal terminals of the s-LN_vs and do not seem to express CRY (Benito *et al.*, 2008; Yoshii *et al.*, 2008). The arborizations of both DN₂s appear to remain in the dorsal protocerebrum and cross the midline of the brain through the pars intercerebralis, to terminate close to the cell bodies of their contralateral counterparts (Helfrich-Förster, 2005). However, due to the wide expression of the clock drivers available (i.e. *Clk856-GAL4*, Gummadova *et al.*, 2009) and the vast overlap of the fibers of other clock neurons in the SLP, it was impossible to finely trace the neurites of the DN₂s so far.

We used the *Clk206-GAL4* driver in combination with *cry-GAL80* to restrict the expression of Flybow exclusively to the CRY-negative clock neurons, which comprise the DN₂s. Unfortunately, GAL80 was not sufficient to repress GAL4 expression in the CRY-positive s-LN_vs and DN_{1a}s, except for the fifth LN. Consequently, none of the 17 brains analyzed contained individually labeled DN₂s. Nonetheless, since all additionally marked neurons have been described at single-cell resolution in our previous study (Schubert *et al.*, 2018), we were able to specifically assign certain projections to known clock neuronal morphologies and therefore to characterize the unique pattern of the DN₂s. We found two main projections of the DN₂s - one toward the medial brain passing to the contralateral hemisphere, the other projection running laterally. The latter

runs dorsolaterally around the SLP and invades the anterior-lateral part of the AOTU. The loop around the SLP reminds strongly of the projections of the CRY-positive DN_{1p}s described above. Since the staining with the *Clk206-GAL4;cry-GAL80* line was only partly satisfying, we looked for split-Gal4 lines that label specifically the DN₂s.

Indeed, the just described DN₂ projection pattern was confirmed by using a split-GAL4 line that specifically labels one DN₂ and none of the other clock neurons (*R43D03-AD; VT003234*; Sekiguchi *et al.*, 2020, **Supplementary Video S3**) and by the *Clk9M-GAL4* line combined with *Pdf-GAL80*, which has been reported to label one or both DN₂ (Kaneko *et al.*, 2012; Goda *et al.*, 2016). The new split-GAL4 DN₂ driver was considerably weaker than the *Clk206-GAL4* and the *Clk9M-GAL4* driver, but we got satisfying labeling with a cytosolic GFP reporter that accumulates GFP stronger than the membrane-bound GFP does (**Supplementary Table S1**). In the case of *Clk9M-GAL4; Pdf-GAL80*, membrane-bound GFP was sufficient for labeling the DN₂s. As expected, the novel split-GAL4 line marked only one DN₂ and this cell was always CRY-negative (**Figure 10A**). With the *Clk9M-GAL4; Pdf-GAL80*, we could see two DN₂s in only one brain (out of 16, **Figure 10B**). In all other brains, again only one DN₂ was labeled, and in about half of the cases, the labeled DN₂ was weakly CRY-positive (**Figure 10B**). This suggests that the two DN₂s can be distinguished by their CRY expression level, and that *Clk9M-GAL4* drives GFP either in the CRY-negative or in a weakly CRY-positive DN₂. Nevertheless, we did not see any difference in morphology between the different individually labeled cells, suggesting that the two DN₂s are very similar. In the following, we will describe the typical morphology of the DN₂s in more detail.

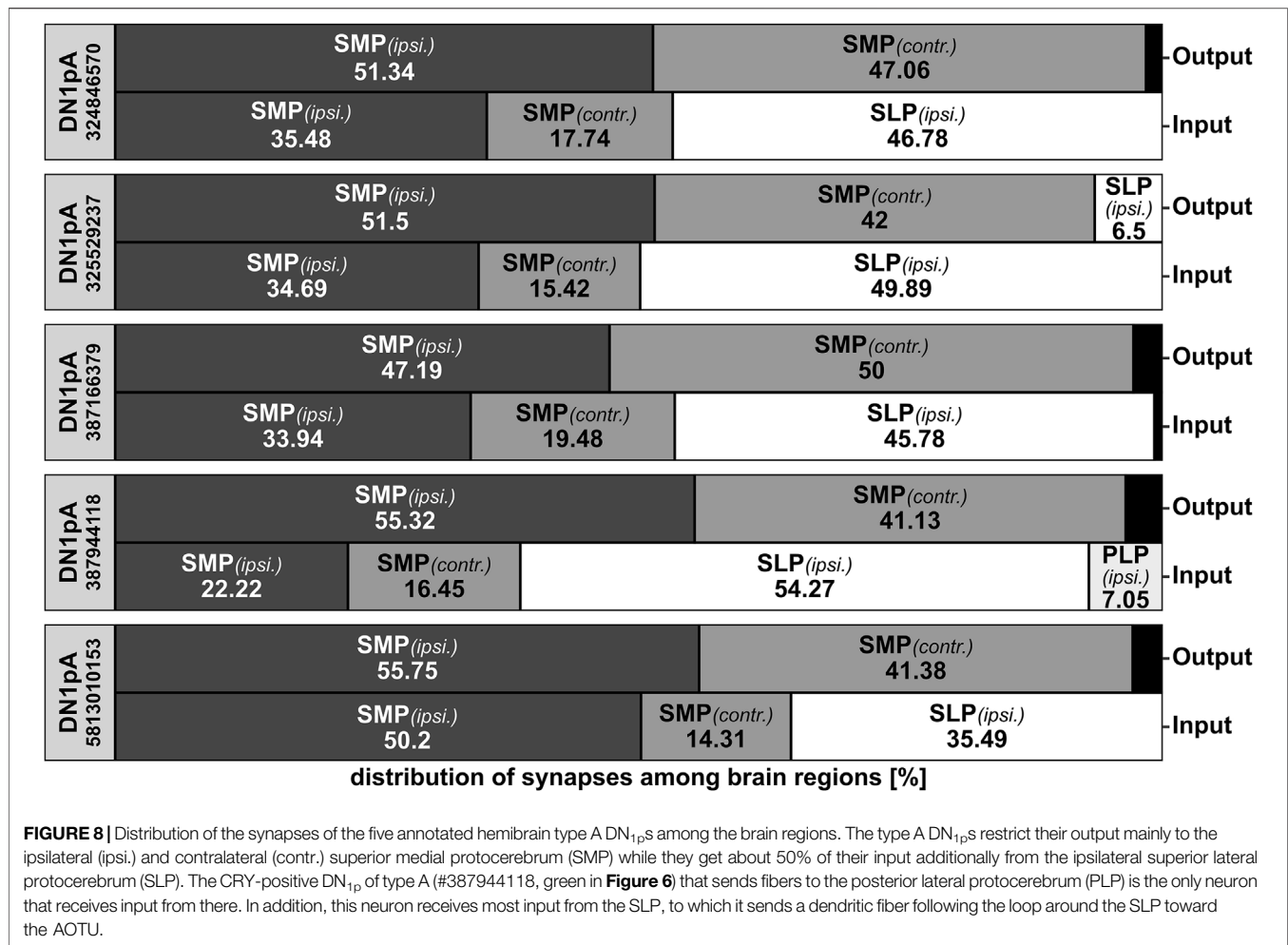
Shortly after leaving the soma, the DN₂ neurites bifurcate into two main branches. As found by Flybow, one runs to the contralateral brain hemisphere (arrow in **Figure 10A**), the other runs laterally (green arrowhead). The laterally running branch projects into the dorsal SLP and then runs further anteriorly forming the characteristic loop around the SLP toward the AOTU, but the DN₂ fibers do not reach it (**Figures 10–12**). Often this branch splits into two prominent fibers (**Figure 11A**). Before the split-off of the lateral branch(es), some less intensively stained fibers turn ventrally and follow the PDF-positive s-LN_v terminals for several micrometers (**Figure 10**, green double arrowheads). Generally, the ipsilateral remaining DN₂ fibers were in close vicinity to the s-LN_v terminals, suggesting an interaction between the two clock neuron types (*see also below*). In one case (out of 15 brains), fibers of the s-LN_v terminals even followed the dorsolaterally projecting DN₂ fibers (magenta arrowhead in **Figure 11A**). The contralaterally projecting fibers of the DN₂s showed



pronounced varicosities and terminated in the superior protocerebrum slightly before they reached the contralateral DN₂ somata (white double arrowheads in **Figures 10A, 11A**). Sometimes we saw fine non-varicose fibers extending from the

varicose fibers further laterally (open double arrowhead, **Figure 10A**).

The arborizations of the DN₂s did not only largely overlap with the PDF-positive fibers of the s-LN_s but also with those of



the ITP-positive fibers from the fifth LN and LN_d (**Figure 11B**). This was especially true in the SMP to SLP, in which the arborizations of the ipsilateral DN₂s were less varicose than those running to the contralateral hemisphere. As for ITP-positive clock neurons, the close vicinity to the DN₂s was maintained throughout the SMP where both clock neuron types cross the midline of the brain in the MDC (**Figure 11B**).

Synapses and Putative Synaptic Partners of the DN₂s

So far, the neuromessengers used by the DN₂s are unknown. The prominent varicosities in the contralaterally projecting terminals of the DN₂s suggest modulatory neuropeptides that are released *via* volume transmission, but the DN₂s may additionally utilize fast neurotransmitters operating *via* synapses. Single-cell transcriptome data (Ma et al., 2021) proposed glutamate as a neurotransmitter of the DN₂s, but glutamate was not detected in the DN₂s by immunohistochemistry (Hamasaka et al., 2007). Our polarity assessment by Synaptobrevin::EGFP and Denmark shows that the DN₂s are strongly polarized (**Figures 12B,C,E**). They receive input in the ipsilateral brain hemisphere and have output synapses at the contralateral

hemisphere. A very similar distribution of synapses was also found in neuron #477918443 of the hemibrain (**Figures 12E, 13B**). This neuron morphologically largely resembles the two DN₂s (**Figure 12D** and **Supplementary Video S3**). As revealed by our polarity staining most input synapses are found on the DN₂ fibers projecting anteriorly around the SLP toward the AOTU. These DN₂ fibers largely intertwine with presynaptic fibers from the CRY-positive DN_{1p}s (**Figure 11C**, double arrowhead), suggesting that the latter signal to the DN₂s, an assumption that is strongly supported by the high number of output synapses from the CRY-positive DN_{1p}s to the DN₂s (**Figures 9A, 13A**). The only other clock neurons giving input to the DN₂s are the s-LN_vs (**Figure 13A**). This supports the findings of Tang et al. (2017) who could find putative synaptic contact between the s-LN_vs and the DN₂s using GFP Reconstitution Across Synaptic Partner (GRASP) (Tang et al., 2017).

Trans-Tango staining with the split-GAL4 and *GAL4/GAL80* DN₂ lines turned out to be more equivocal than for the other clock neurons. This was the case because the *R43D03-AD; VT003234* split-GAL4 line was such a weak

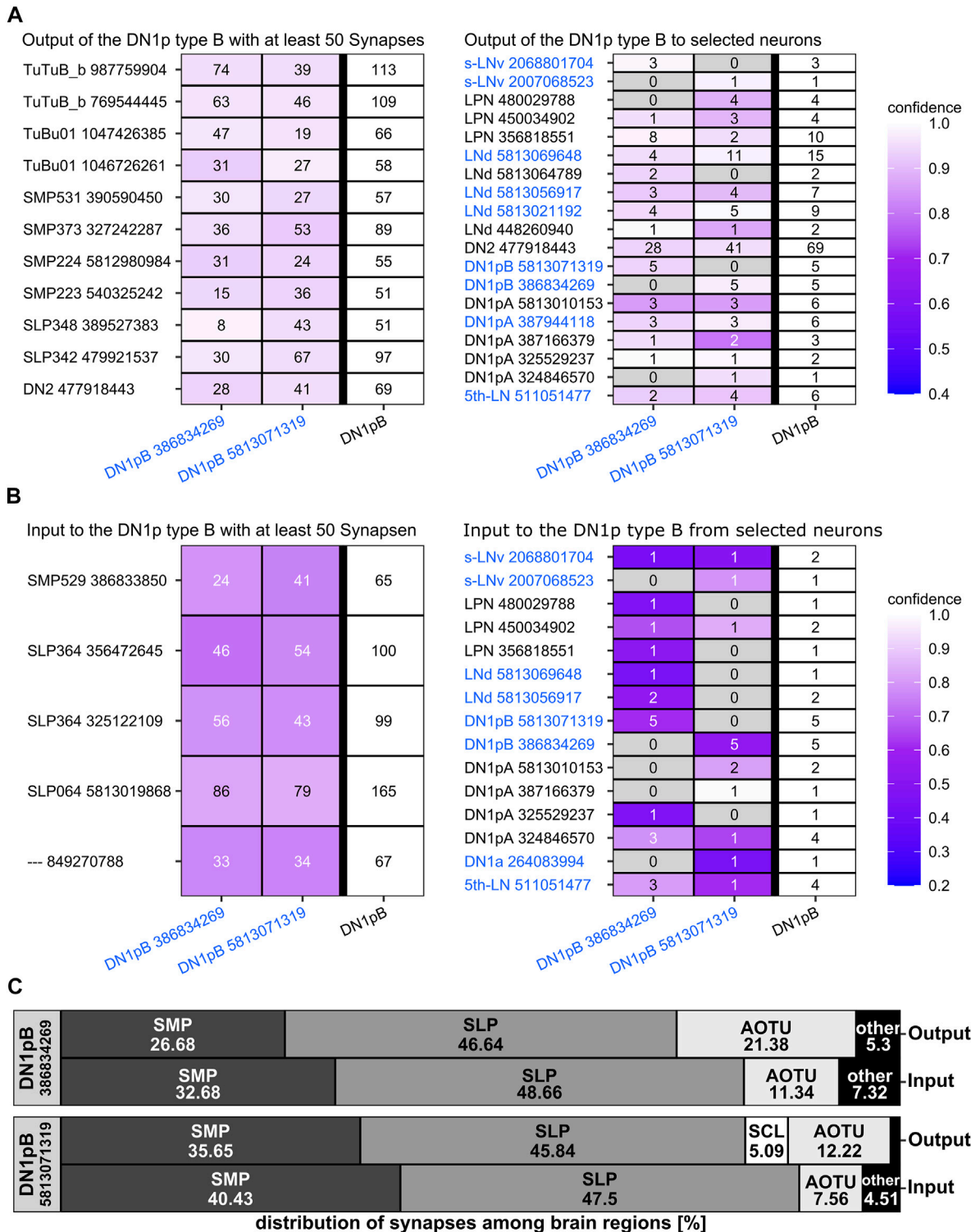
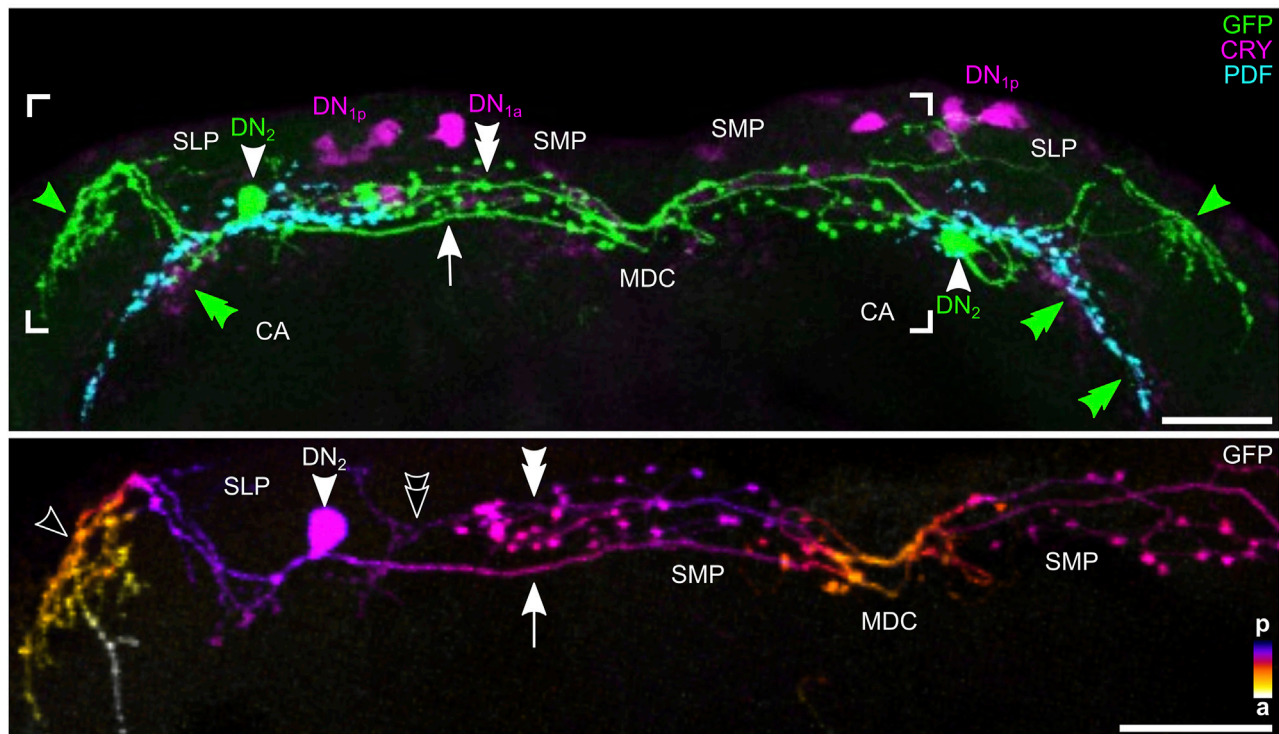


FIGURE 9 | Synaptic partners of the two annotated CRY-positive type B DN_{1p}s from the hemibrain. **(A)** Postsynaptic partners of the CRY-positive type B DN_{1p}s with at least 50 synapses and postsynaptic clock neurons. As expected, the DN_{1p}s project on many tubercle bulb neurons (TuBu) of the anterior optic tubercle (AOTU) and to tubercle-tubercle neurons (TuTuB) which are connecting the AOTUs of both hemispheres. Additionally, neurons with their cell bodies in the superior lateral protocerebrum (SLP) as well as in the superior medial protocerebrum (SMP) get strong input by the CRY-positive type B DN_{1p}s. Further, they give strong input to one DN₂ as the only clock neuron which is getting strong input from the type B CRY-positive DN_{1p}s. Other clock neurons like the LPN and the type A DN_{1p}s get only weak input from the CRY-positive DN_{1p}s. **(B)** As the CRY-positive DN_{1p}s give output to neurons of the SMP and SLP they also do get strong input by neurons from these brain (Continued)

FIGURE 9 | regions. Interestingly they do not seem to receive synaptic input from the clock network. **(C)** Distribution of the input and output synapses of the CRY-positive DN_{1p}s among the brain regions. The neurons form most of their synapses in the SMP, AOTU, and SLP with most synapses in the latter. The number of input and output synapses are similar in the different brain regions, but the two DN_{1p}s slightly differ in the percentage of output synapses in the SMP and AOTU. DN_{1p} #5813071319 has more input and output in the SMP and less input and output in the AOTU than DN_{1p} #386834269. In addition, DN_{1p} #5813071319 is the only so far annotated DN_{1p} that has output in the superior clamp (SCL). Note that the two Type B DN_{1p}s do not receive significant input from the PLP, although they send fibers into this region.

A *R43D05-p65.AD; VT003234-DBD>20xUAS-6xGFP*



B *clk9M-Gal4; pdf-Gal80>myrGFP*

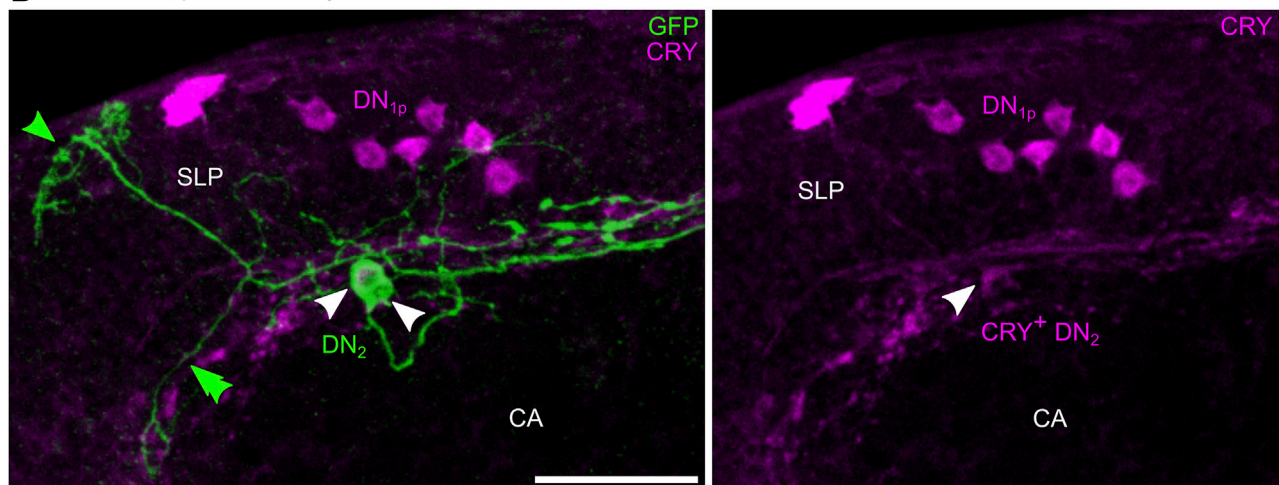


FIGURE 10 | The morphology of the DN₂s. **(A)** Maximal projection of 20 confocal planes showing a frontal view of the dorsal protocerebrum, in which one DN₂ is marked with cytosolic GFP using the split-GAL4 line *R43D03-AD; VT003234* with the *20xUAS-6xGFP* reporter) and counter-stained with anti-CRY (magenta) and anti-PDF (cyan). The lower panel shows the GFP labeling of the area marked above in greater detail in color-coded depth information. Fibers in the posterior (p) brain are marked blue and fibers further anterior (a) are marked in yellow/white. **(B)** Maximal projection of 26 confocal planes showing a frontal view of the left dorsolateral protocerebrum, in which two DN₂s are marked with membrane-bound GFP (using *Clk9M-GAL4; Pdf-GAL80* with the *UAS-myrGFP* reporter) and counter-stained with anti-CRY (magenta). Note that one of the two DN₂s is weakly CRY-positive (CRY⁺ DN₂, right). Green arrowheads mark the DN₂ fibers projecting to the anterior optic (Continued)

FIGURE 10 | tubercle (AOTU), green double arrowheads mark fibers that follow the PDF terminals for several micrometers ventrally, green arrows point to the DN₂ fiber running contralaterally, and thick green arrows to the varicose terminals on the contralateral side. From these, in some cases, weak, nonvaricose fibers continue toward the contralateral soma of DN₂. MDC, middle dorsal commissure; CA calyx of the mushroom bodies. Scale bars represent 50 μm.

driver that we could not detect the DN₂s in the presynaptic GFP channel, making it therefore difficult to trust the postsynaptic staining. The *Clk9M-GAL4; Pdf-GAL80* line, on the other hand, showed sometimes expression in the DN_{1a}s that made us doubt that we can rely on all postsynaptic labeling we saw. Nevertheless, both drivers led consistently to HA-expression in Kenyon cells of the mushroom bodies and all their lobes (**Figure 11D**). Since the DN_{1a}s do not signal onto the mushroom bodies and the DN₂s neurites project close to the calyces of the mushroom bodies, it is quite likely that they indeed form synapses with specific Kenyon cells. In addition, in the stronger *Clk9M-GAL4; Pdf-GAL80* line, we found always postsynaptic labeling in the pars intercerebralis. In several brains, few neurosecretory cells of the pars intercerebralis were labeled, projecting through the median bundle down to the esophageal foramen and the subesophageal zone (**Figure 11D**). Since the neurites of the DN₂s cross the midline of the brain at the exact location where we see dense HA labeling (arrow in **Figure 11D**), this staining pattern is likely true and the DN₂s do indeed form synapses with neurosecretory cells of the pars intercerebralis.

It is also important to note that we did not see any postsynaptic staining in any of the clock neurons, suggesting that the DN₂s might not form any output synapses with other clock neurons. In the hemibrain, no output synapses of the DN₂ (#477918443) were annotated, because the latter are found on the contralateral hemisphere. Input to the DN₂s came mainly from the ipsilateral SLP and here mainly from the CRY-positive DN_{1p}s (**Figure 13**).

The DN₃s

Comprising approximately 40 cells, the DN₃s are by far the largest clock neuron cluster in the brain of the adult fly. Several studies have already revealed the presence of larger and smaller DN₃ cell bodies, and that some of them are situated more anteriorly in the brain compared to the others (Helfrich-Förster, 2003; Shafer et al., 2006; Helfrich-Förster et al., 2007b). This is in line with our observations made on 43 brains, in which the Flybow-reporters were expressed under the control of the pan-clock-neuronal *Clk856-GAL4* driver. The somata of approximately 15 DN₃s are located posterior to the LH, whereas the remaining cells reside more anteriorly in the dorsal and lateral cell body ring of the LH, respectively. The majority of DN₃s possess rather small cell bodies and only about four to five neurons have larger somata. Half of the larger cells are found among the small posterior DN₃s, while the other two are found among the more anteriorly located neurons of this group. Interestingly, the projections of the large DN₃s strongly resemble the

arborization pattern of the ITP- and CRY-positive LNs (fifth LN and LN_d) (Schubert et al., 2018). Their projections initially run along the posterior boundary between the LH and the SLP (**Figures 14A,B** open arrowhead). The first branching occurred on the posterior surface of the brain at the level of the trijunction between the LH, SLP, and SCL (**Figures 14A,B**, arrows). Here, some of the fibers from the large DN₃ projected anteriorly to the AOTU *via* three paths. The fiber bundle running along the first path, projects around the surface of the SLP. This is the same path (or better loop) used by the CRY-positive DN_{1p}s and the DN₂s projecting towards the AOTU. The second path towards the AOTU coincides with the second loop of the CRY-positive DN_{1p}s that runs along the trijunction of SLP, SCL, and superior intermediate protocerebrum. The third path originates in the lateral PLP and runs along the surface of the anterior ventrolateral protocerebrum. These different fiber bundles running in the different paths are hard to identify in **Figure 14** (anterior projecting fibers in yellow) and are best seen in **Supplementary Video S4**.

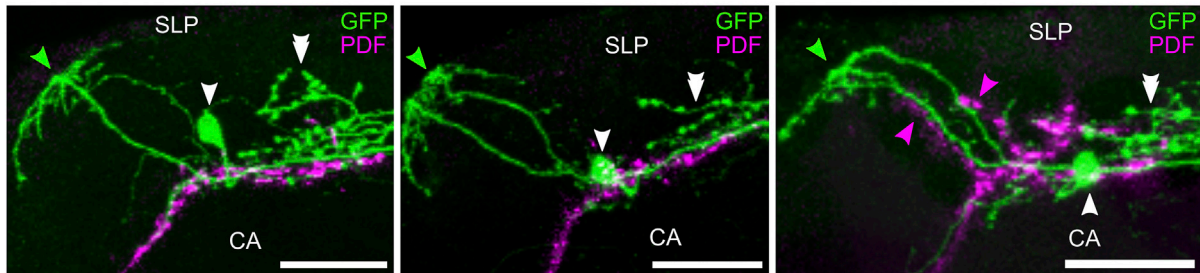
Other fibers of the DN₃s remained initially posterior (blue colors in **Figure 14A**) and passed ventrally through the PLP until they reached the ipsilateral AME (**Figure 14A** white double arrowhead). On their way to the AME, numerous side-branches separated from the main bundle and formed a kind of fiber hub (**Figure 14A** double open arrowhead) where they overlap with the ITP- and CRY-positive LNs (*see Supplementary Video S5*).

Most fibers of the DN₃ projected medially forming a dense varicose fiber network in the SMP (**Figures 14A,B**, arrowheads). From there, a portion of the projections crossed the midline of the brain *via* the MDC and superior arch commissures (SAC) reaching into the contralateral hemisphere (**Figures 14A,B**).

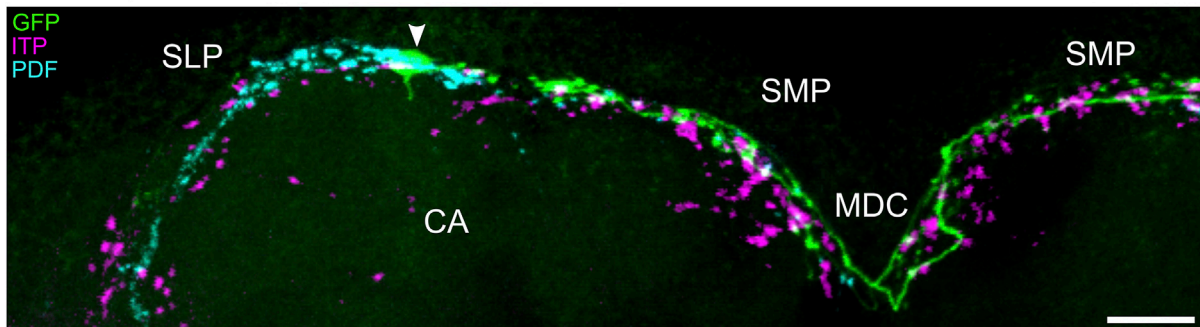
We observed a different arborization pattern in brains in which only the small DN₃s were labeled compared to brains in which both, the large and small DN₃s were stained (**Figure 14B**). In these brains, the two hemispheres were connected exclusively *via* the MDC, with no additional projections through the SAC (**Figure 14B**). However, there are even more apparent differences between the small and large DN₃s: the small DN₃s lack the fiber bundle towards the AOTU and the projections ending in the AME. The fibers of the small DN₃s, that pass through the PLP toward the AME terminate in the fiber hub of the PLP halfway to the AME described above (**Figure 14B** double arrowheads). Thus, only the four to five large DN₃s send fibers into the AOTU and AME (**Figure 14C**).

No DN₃s could be annotated with certainty in the hemibrain dataset until now. However, there are possible candidates available of which three subtypes can be distinguished. While two subtypes comprise only five (named DN₃) and six (named

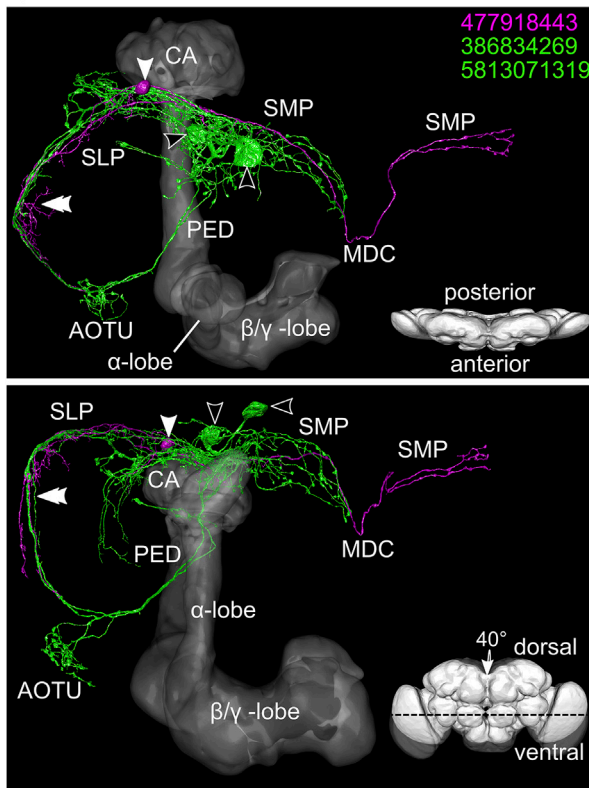
A *R43D05-p65.AD; VT003234-DBD> 20xUAS-6xGFP*



B *R43D05-p65.AD; VT003234-DBD> 20xUAS-6xGFP*



C



D *clk9M-Gal4; pdf-Gal80>trans-Tango*

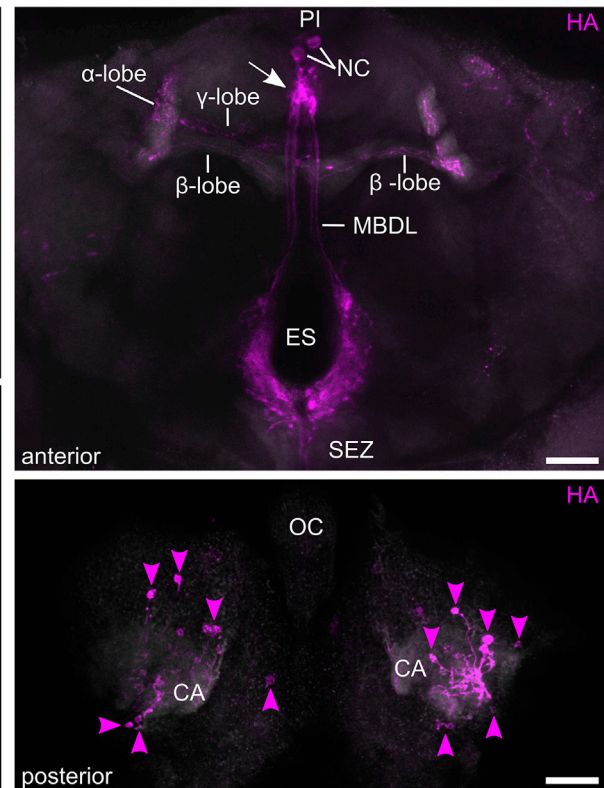


FIGURE 11 | Vicinity of the DN₂s to other clock neurons and putative downstream synaptic partners. **(A)** Confocal images (overlay of 27, 43, and 21 stacks, respectively) demonstrating the close vicinity of the DN₂s (green) to the PDF-positive terminals of the s-LN_s (magenta). Labeling as in **Figure 9**. **(B)** Maximal projection of 18 confocal planes showing the close vicinity of the DN₂s (green) to the ITP-positive LN₅ and fifth LN (magenta) and the PDF-positive terminals of the s-LN_s (cyan). White arrows mark the overlap of ITP-positive fibers with the contralateral projecting fibers of the DN₂s in the superior median protocerebrum (SMP) and the middle dorsal commissure (MDC). **(C)** Overlay between DN₂ and CRY-positive DN_{1p} fibers running around the SLP to the anterior optic tubercle (AOTU). **(D)** Neurons postsynaptic to the DN₂s revealed by *trans-Tango*. Top: maximal projection of eight confocal planes from the anterior brain depicting postsynaptic HA staining in neurosecretory cells (NC) running in the median bundle (MBDL) and around the esophagus (ES) to the subsesophageal zone (SEZ) as well as in the α - and β -lobes of the mushroom bodies. (Continued)

FIGURE 11 | The white arrow points to a dense HA-positive fiber net that lies exactly in the midline of the brain where the DN₂s cross in the MDC (compare with **B**). Bottom: maximal projection of four confocal planes from the posterior brain showing postsynaptic staining in Kenyon cells (small magenta arrows) of the mushroom body as well as in the calyces (CA). OC, ocellar tract. Scale bars represent 25 μm.

DN₃B) neurons, respectively, the third subtype comprises 15 neurons (named DN₃A) (**Supplementary Video S4**). Comparing the morphology of these DN₃ candidates with our findings, we are fairly confident that the subtype with five neurons comprises the large DN₃s, as their projection pattern is consistent with our descriptions (**Figure 14D**). The only difference is that there are no fibers reported running through the SAC in the hemibrain that we observed in our Flybow staining, but this might be caused by a general lack of contralateral projections in the hemibrain, which we discussed previously (Reinhard et al., 2022).

The second group of DN₃s candidates from the hemibrain that matches our description is the DN₃A subtype comprising 15 neurons. These neurons largely resemble the small DN₃s. As we found in our staining they project halfway down to the AME and terminate in the PLP fiber hub.

The third subtype of DN₃ candidates in the hemibrain completely lacks the projections extending ventrally towards the AME in the PLP. Otherwise, it looks similar to the small DN₃s. We did not see this subtype in our staining, but most likely, the DN₃s comprise more subtypes than we and others could identify so far.

The small DN₃s were also labeled by Guo *et al.* (2018) as common neurons between the *Clk856-GAL4* and the *R77H08-LexA* driver lines (Guo et al., 2018 Supplementary Figure S1A). Furthermore, Meiselman *et al.* (2022) recently found the large (and several small DN₃s) labeled by a specific split-*GAL4* line. These authors report the same arborization pattern that we describe here. They also found a faint commissure in the superior brain, but unfortunately, we could not distinguish between the SAC and MDC according to their figures (Figure 2K in Meiselman et al., 2022).

Due to the lack of specific driver lines, we have not yet been able to perform a polarity analysis of the DN₃s. It will be most promising to do so in the future with the recently published split-*GAL4* line. In addition, we assume that the hemibrain DN₃ candidates will be certainly annotated as DN₃s as soon as further experiments allow a more accurate comparison in respect of their polarity and synaptic partners.

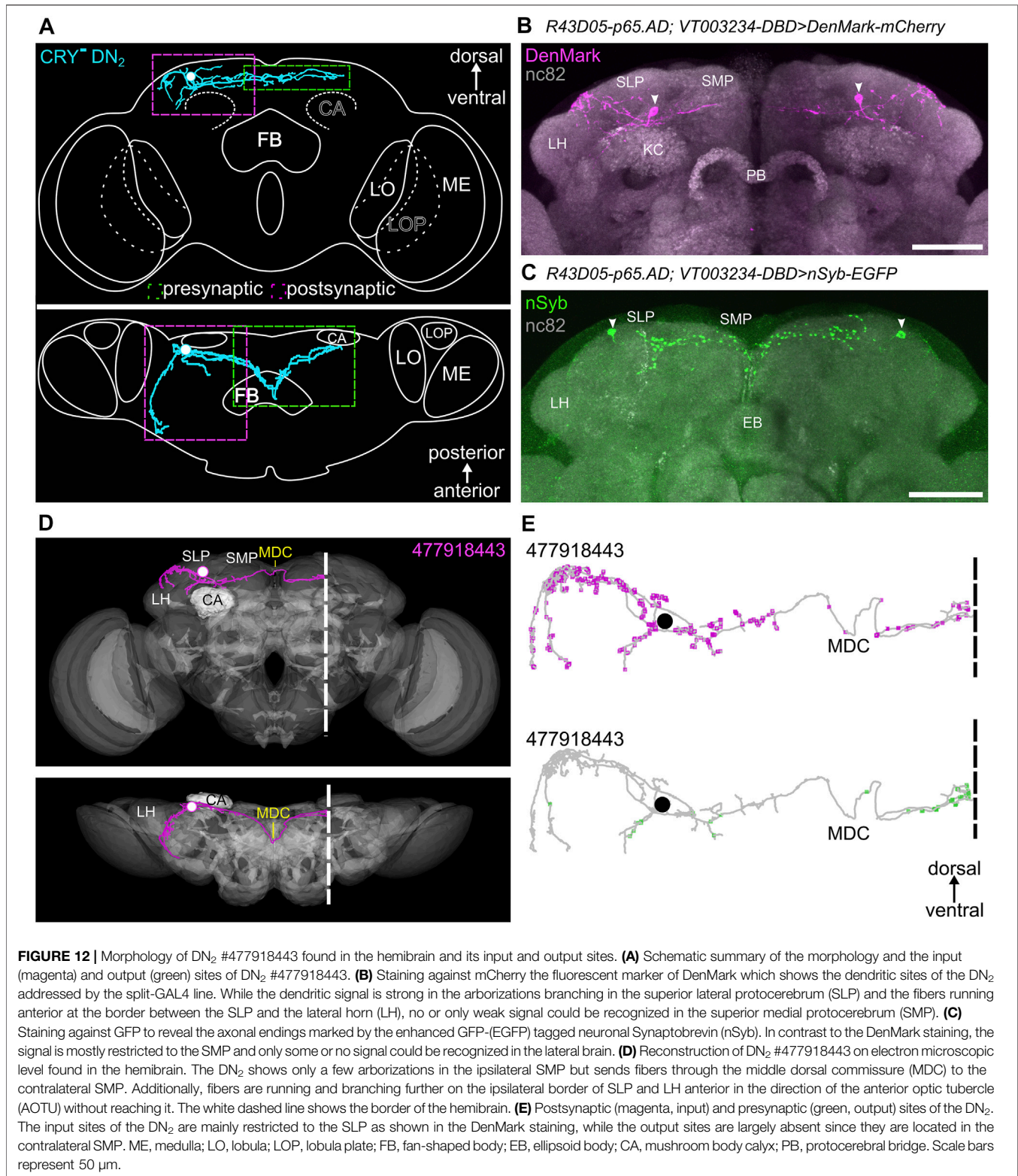
DISCUSSION

This study aimed to unravel the morphology and connectivity of *Drosophila*'s dorsal clock neurons. Throughout the results, we have compared our findings with those of previous studies, which we largely confirm. Nevertheless, we found new details that reveal a so far unknown degree of heterogeneity within certain clock neuron groups that might impact their function. Only the two DN_{1a}s and two DN₂s appear to have similar morphology. This observation is

supported by single-cell RNA sequencing analysis that found no qualitative differences within the neurons of these groups (Ma et al., 2021). At the same time, the DN_{1a}s and DN₂s (together with the four s-LN_vs and the fifth LN) are functional from the first larval instar onward making them basic clock neurons that might be of particular functional importance (Kaneko et al., 1997). In the following, we will discuss our findings in the light of numerous functional studies that have attributed specific roles to the clock neuron groups, with a special emphasis on the DN_{1a}s and DN₂s.

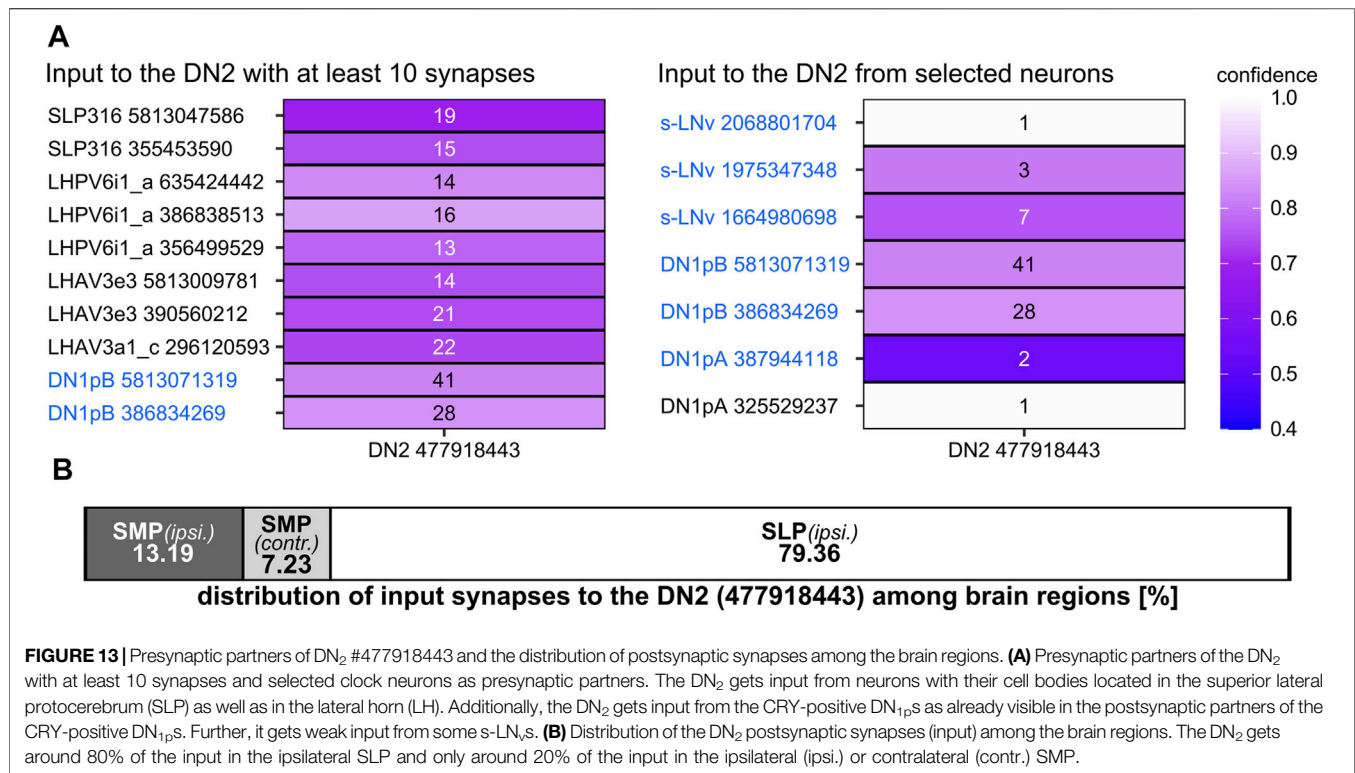
Putative Functional Impact of the DN_{1a}s

The DN_{1a}s express two neuropeptides (CCHamide1 and IPNamide) (Shafer et al., 2006; Fujiwara et al., 2018) and one neurotransmitter (glutamate) (Hamasaka et al., 2007). They are functionally strongly interconnected with the s-LN_vs *via* neuropeptide signaling. While the s-LN_vs signal to the DN_{1a}s *via* PDF (Shafer et al., 2008; Im et al., 2011), the DN_{1a}s signal to the s-LN_vs *via* CCHamide1 (Fujiwara et al., 2018). Here, we show by *trans*-Tango that the two neurons are additionally interconnected *via* regular synapses. This fits with previous *trans*-Tango studies (Song et al., 2021) as well as immunohistochemical results demonstrating that the s-LN_vs express metabotropic glutamate receptors that can be activated by glutamate from the DN_{1a}s (Hamasaka et al., 2007). *Vice versa*, the DN_{1a}s might express glycine receptors that can be activated by glycine released from the s-LN_vs, although this has not yet been proven (Frenkel et al., 2017). Manipulations of the reciprocal peptidergic connections between the DN_{1a}s and the s-LN_vs affect the flies' free-running period, their morning and evening activity as well as their siesta under light-dark conditions (Fujiwara et al., 2018). The synaptic connections between the two neuron groups have not been specifically manipulated, but the knockdown of glutamate receptors in the s-LN_vs increases the free-running period and the nocturnal activity under light-dark conditions (Hamasaka et al., 2007). Furthermore, downregulation of glutamate synthetase in all dorsal clock neurons increases the rhythmicity of flies under constant light conditions (de Azevedo et al., 2020), indicating that glutamate signaling from the DN_{1a}s is involved in the general light sensitivity of the clock. Although it is unlikely that this effect is mediated exclusively by the DN_{1a}s (some DN_{1p}s and DN₃s are also glutamatergic as shown by Hamasaka *et al.* (2007) and Collins *et al.* (2012)), the DN_{1a}s appear to contribute strongly to the light detection. At night, their silencing reduces light-induced startle responses, whereas during the day, PDFR-dependent signaling to the DN_{1a}s limits light-induced startle responses (Song et al., 2021). As we show here, the DN_{1a}s get strong input from the dorsal and lateral accessory calyces. The dorsal accessory calyces transfer visual information from the lobula (Li et al., 2020). Thus, DN_{1a}s may directly receive light information from the optic lobe.



On the other hand, the lateral accessory calyces convey thermosensory information from neurons in the antennal lobes (Marin et al., 2020). While about half of the clock

neurons are intrinsically light-sensitive (*via* CRY), none of them is per se temperature-sensitive (Sehadova et al., 2009) but they rely on temperature input from peripheral sensory



neurons (the arista on the antennae, the chordotonal organs and the antennal AC neurons (Tang et al., 2017; reviewed in; George and Stanewsky, 2021)). Indeed, the DN_{1a}s get strong synaptic input from several temperature sensing projection neurons from the antennal lobes. Alpert et al. (2020) showed that temperatures below the preferred temperature for flies (~25°C) silence the DN_{1a}s via GABAergic synapses from such thermosensory projection neurons. This silencing leads to reduced activity and increased sleep in the morning and evening, which can only be overwritten by light and PDF signaling. Indeed, we found that the DN_{1a}s signal not only to the morning neurons (the s-LN_vs) but even stronger to the evening neurons, namely the CRY- and ITP-positive fifth LN and LN_d. In addition, the DN_{1a}s have few output synapses to tangential neurons arborizing in the second and eighth layer of the dFB, which overlap with the fibers of several clock neurons in the PLP. The dFB is known to be involved in the control of sleep (reviewed in Bertolini and Helfrich-Förster, 2021).

Altogether these results demonstrate that the DN_{1a}s play a central role in light- and temperature integration of the circadian clock and can prominently influence the morning and evening neurons as well as the sleep of flies.

Putative Functional Impact of the DN_{1p}s

We could show that the DN_{1p}s consist of more than the originally described two types of CRY-positive and CRY-negative neurons. In the hemibrain, seven of the ~15 DN_{1p}s are annotated. The seven neurons are classified into type A and type B neurons, but the type A neurons appear heterogeneous. At least one type A neuron looks

different from the others (green neuron in Figure 6). We found the same neuron type by Flybow and identified an additional one that was not yet annotated in the hemibrain. Lamaze et al. (2018) depict a further DN_{1p} type in their supplement that was neither identified in the hemibrain nor in the present study. These two previously undescribed DN_{1p}s project contralaterally like the type A neurons but differ in their projections toward the AOTU and PLP. The DN_{1p} identified here lacks the anterior projections to the AOTU but shows prominent fibers to the PLP (Figure 6D right panel), whereas the DN_{1p} identified by Lamaze projects anteriorly to the AOTU and lacks fibers in the PLP (Supplementary Figure S1A in Lamaze and Stanewsky, 2020). These findings demonstrate that the DN_{1p}s encompass many neurons with different morphology and most likely also different neurochemistry. Single-cell RNA sequencing data underline this conclusion: according to their gene expression, the DN_{1p}s comprise five to six distinct clusters (Ma et al., 2021). This heterogeneity could explain the different and partly contradicting findings regarding their function(s) (reviewed in Lamaze and Stanewsky, 2020). We will not repeat these details here but instead, focus on the main findings adding new insights that derive from the present study.

The DN_{1p}s appear to comprise morning and evening neurons (Chatterjee et al., 2018), which is strongly supported by our findings. Type A DN_{1p}s receive strong synaptic input from the evening neurons (ITP positive fifth LN and LN_d) and signal even stronger back to them. Thus, there exists a prominent mutual connection between the type A DN_{1p}s and the evening neurons, suggesting that the five annotated type A DN_{1p}s are by themselves evening neurons. Nevertheless, the seven neurons are heterogeneous and at least one of them (green

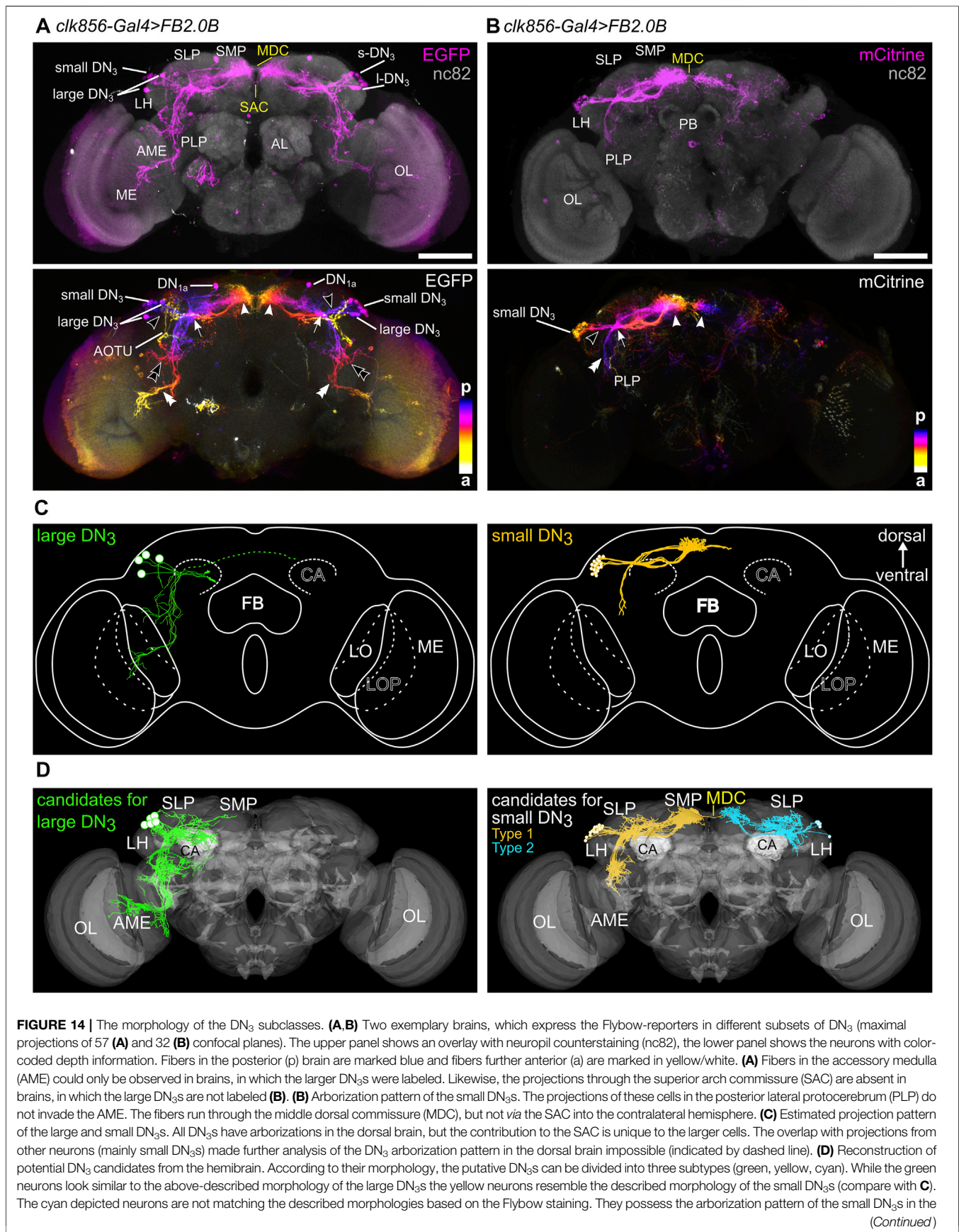


FIGURE 14 | superior lateral protocerebrum (SLP) but lack the fibers projecting ventrally to the posterior lateral protocerebrum (PLP). These neurons could be a further subtype of the DN₃s, which was not detected by the Flybow staining. Candidates for the large DN₃: #510602264, #5813021221, #356140100, #5813057153, #5813020750; candidates for (DN₃) small DN₃ type 1: #357949102, #5813010377, #358285424, #358976515, #450371612, #478937243, #510680957, #571364144, #664447502, #5813026780, #5813032640, #451424866, #574062996 (DN₃_A). Candidates for small DN₃ type 2: #326465302, #356835277, #386847799, #417536905, #417882515, #479260921, #358631450, #328273806 (DN₃_B). LH, lateral horn; ME, medulla; LO, lobula; LOP, lobula plate; FB, fan-shaped body; EB, ellipsoid body; CA, mushroom body calyx; PB, protocerebral bridge; AL, antennal lobe. Scale bars represent 50 μm.

neuron in **Figures 5, 6**) gets synaptic input in the PLP, a region where many clock neurons arborize. This DN_{1p} may additionally receive input from morning neurons (s-LN_vs) *via* PDF or from the LPNs *via* DH31 (Reinhard et al., 2022). So far this is the only annotated type A DN_{1p} neuron that is most likely CRY-positive, expresses the PDF receptor and additionally receives synaptic input in the PLP. It is tempting to speculate that all DN_{1p}s that overlap with the s-LN_v projections in the PLP are CRY-positive, but this has to be proven by future studies. The type B DN_{1p}s are all CRY-positive, largely overlap with projections from the s-LN_vs, and express the PDFR. Thus, they are connected *via* PDF with the morning neurons and can contribute to the morning activity of the flies.

At the same time, DN_{1p}s consist of sleep- and activity-promoting neurons (Guo et al., 2018; Lamaze et al., 2018). Through their fibers projecting to the pars intercerebralis, they affect wakefulness by signaling to neurosecretory cells expressing the *Drosophila* homolog of the mammalian corticotropin-releasing factor (Cavanaugh et al., 2014; Kunst et al., 2014). In contrast, the anterior projections of the DN_{1p}s to the AOTU, appear to play a prominent role in sleep control because in the AOTU, CRY-positive type B DN_{1p}s signal on sleep-promoting ring neurons of the ellipsoid body, influencing their neuronal activity (Lamaze et al., 2018). Here, we could confirm the intimate connection of the DN_{1p}s to the AOTU. Moreover, we could show that the projections of the DN_{1p}s toward the AOTU largely overlap with fibers from the DN₂s and large DN₃s. The DN_{1p}s strongly signal *via* these projections to the DN₂s (*see* below).

DN_{1p}s are also known to promote the siesta of the flies (Guo et al., 2016) and to inhibit activity at low temperatures (Yadlapalli et al., 2018). They respond to cool temperatures (~16°C) with a strong increase in firing rate, while they are inactive at warm temperatures (>25°C) (Yadlapalli et al., 2018). In contrast to the DN_{1a}s, the DN_{1p}s do not arborize in the lateral accessory lobes, but they seem to receive temperature information from thermoreceptors in the arista of the antennae and chordotonal organs in the body *via* signals from anterior cells (AC) which are known to be involved in temperature sensing pathways (Hamada et al., 2008; Yadlapalli et al., 2018; Jin et al., 2021). Thus, the DN_{1p}s appear to be a major gateway for temperature sensing into the circadian neural network, which continuously integrates temperature changes to coordinate the timing of sleep and activity. Most likely, the DN_{1p}s pass this information to other clock neurons, which do not receive temperature input directly but are similarly involved in temperature-related behavior (e.g. DN₂, Kaneko et al., 2012; Goda et al., 2016).

It is worth noting that the so far annotated type A DN_{1p}s are quite polar and have their synaptic output sites in the contralateral SMP. The same is true for the DN₂s, which we will discuss in the following.

This feature might be important for integrating information from both hemispheres.

Putative Functional Impact of the DN₂s

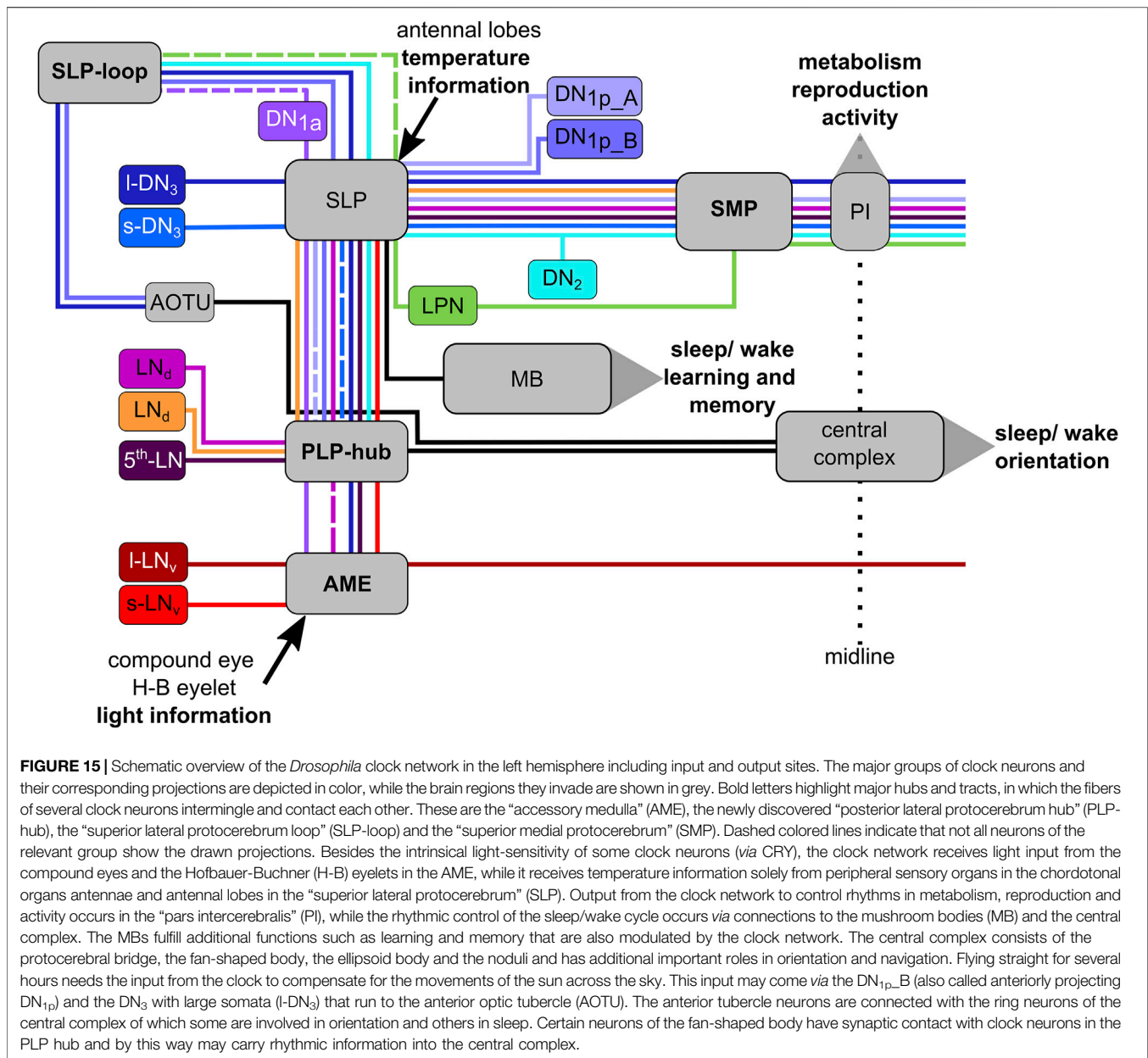
The two DN₂s, similarly to the DN_{1a}s, show a special association with the s-LN_vs. All three clock neuron groups express PER cyclically already during the larval stages, whereas PER in the larval DN₂s cycles in antiphase to the other clock neurons (Kaneko et al., 1997). This anti-phase cycling depends on PDF signaling from the s-LN_vs to the DN₂s (Picot et al., 2009) suggesting that the DN₂s are PDFR positive, although they are reported to be CRY-negative in adults (Benito et al., 2008; Yoshii et al., 2008). Here, we report weak CRY-immunostaining in one of the DN₂s, strongly suggesting that the PDFR is also present since they are always co-expressed (Im et al., 2011).

The DN₂s are important for temperature entrainment in larvae (Picot et al., 2009) and temperature preference in adults (Kaneko et al., 2012). In contrast to the DN_{1a}s, the DN₂s do not arborize in the lateral accessory calyces and we could not detect any direct input from temperature sensing neurons of the antennal lobes. Nevertheless, the DN₂s could get information indirectly *via* other clock neurons. The most promising candidates are the type B CRY-positive DN_{1p}s that get input from thermosensory AC neurons and that strongly contact the DN₂s. Furthermore, Tang et al. (2017) suggested that AC neurons project also directly to the DN₂s. In addition to synaptic input, the DN₂s may receive neuropeptidergic input from the DN_{1p}s *via* DH31 (Goda et al., 2016).

The DN₂s themselves do barely signal to other clock neurons, suggesting that they are pure output neurons of the clock network. As mentioned, they are highly polar as they receive synaptic input in the ipsilateral SLP and have output synapses in the contralateral SMP. As we show here by *trans*-Tango, their main output sites are the mushroom bodies and neurosecretory cells in the pars intercerebralis. These two sites are highly involved in the regulation of sleep, arousal, and metabolism (*see* above and discussion in Reinhard et al. (2022)). Consequently, DN₂s can impact both processes and adapt them to different environmental temperatures.

Putative Functional Impact of the DN₃s

The DN₃s are the largest and, until very recently, also the less well-characterized group of the dorsal neurons. They are heterogeneous, not only regarding their size and morphology but also in respect to their gene expression, which divides them into two clusters (Ma et al., 2021). Here, we confirm previous findings that the DN₃s consist of neurons with large and small



somata with different morphologies, but they may be composed of further subgroups, as suggested by data from the hemibrain.

Some (~4) of the DN₃s express a homolog of the vertebrate circadian gene *nocturnin*, coding for a deadenylase involved in mRNA decay (Nagoshi et al., 2010), and up to 17 DN₃s express the gene *quasimodo*, coding for a Zona pellucida domain protein (Chen et al., 2011; Buhl et al., 2016). Both proteins are involved in the light perception of the clock. Other observations suggest an additional role of the DN₃s in the sensory integration of temperature cues into the circadian system (Harper et al., 2016). Consistent with this observation, up to 10 DN₃s neurons express the DH31 receptor, and together with the DN₂s cells, they appear necessary for regulating the temperature preference of the flies at the beginning of the night (Goda et al., 2016). The large DN₃s are

additionally responsive to PDF (Shafer et al., 2008). Furthermore, some DN₃s express glutamate, and the majority of them express the neuropeptide AstC (Guo et al., 2018; Díaz et al., 2019; Meiselman et al., 2022). Díaz et al. (2019) suggest that the AstC-positive DN₃s signal to at least one LN_d and in this way influence the evening activity of the flies. Guo et al. (2018) demonstrate a sleep-promoting role of the DN₃s, especially of the small DN₃s. Meiselman et al. (2022) show that the AstC-positive DN₃s regulate the cold-induced dormancy of the flies, supporting the role of the DN₃s in temperature-dependent behavior.

All these different roles are supported by morphological data. Especially the arborizations of the large DN₃s reach the entire clock network. They form arborizations in all four fiber hubs of the clock network (AME, SMP, ventral PLP and the loop in the SLP). In the

AME they might not only receive light input (Li et al., 2018) but also communicate with all lateral neurons. In the SMP, they overlap with all clock neurons besides the LN_{ν} s. In the ventral PLP hub (double open arrowhead in **Figure 14A**) their fibers largely overlap with the cell bodies of the LPNs and with fibers from the evening neurons (ITP-positive fifth LN and LN_d) and the small DN_{3s} . In the SLP loop, they are again in close contact with the evening neurons as well as with many DNs. Consequently, they may communicate with all these neurons. From our *trans*-Tango data, we already know that one to two larger DN_{3s} get input from the DN_{1a} s. Connectivity data from the hemibrain suggest weak synaptic input from the type B CRY-positive DN_{1p} s to some of the small DN_{3s} . The large DN_3 even appear to have dense arborizations in the lateral accessory calyces, which would predispose them to receive information from the thermosensory neurons of the antennal lobes. Moreover, they cross the midline of the brain in two commissures, meaning that they can integrate information from both brain hemispheres. The small DN_{3s} form a prominent fiber network in the SLP and SMP and run ventrally in the PLP where most of them appear to terminate in the fiber hub formed by the arborizations of the large DN_{3s} , fifth LN, and LN_d . Thus, they contribute to the wide connectivity of the large DN_{3s} within the clock network.

CONCLUSION

Here, we show that the DNs are an integral part of the clock network. Functionally, they appear to integrate light and temperature information into the clock network and contribute to the control of many behavioral outputs reaching from sleep and activity to the control of metabolism *via* the neurosecretory system of the fly (summarized in **Figure 15**). Anatomically, we show that the fibers of the DNs intermingle with those of the LNs (**Supplementary Video S5**). Besides the already known AME and the SMP (often referred to simply as the dorsal protocerebrum), we identify two areas in the brain, in which the interplay between all clock neurons appears especially intimate. The first area is the SLP, where several clock neurons join a fiber tract, which forms a loop around the SLP and terminates in the AOTU. These are the CRY-positive type B DN_{1p} s, the DN_{2s} , the large DN_{3s} , the LPNs, and the ITP- and CRY-positive fifth LN and LN_d . The second area lies in the PLP very close to the cell bodies of the LPNs, where the s - LN_{ν} s pass through and the large and small DN_{3s} , the DN_{1a} s, and the ITP- and CRY-positive fifth LN and LN_d contribute to a fiber hub. These two brain areas may serve as additional communications centers for the clock neurons. They may also serve as additional input and output centers of the clock. Here, we show that the clock network signals to certain dFB neurons *via* the PLP hub and Kind *et al.*

REFERENCES

Abruzzi, K. C., Zadina, A., Luo, W., Wiyanto, E., Rahman, R., Guo, F., et al. (2017). RNA-seq Analysis of Drosophila Clock and Non-clock Neurons Reveals Neuron-specific Cycling and Novel Candidate Neuropeptides. *Plos Genet.* 13, e1006613. doi:10.1371/journal.pgen.1006613

(2021) have recently demonstrated connections from the visual system to the AME and the PLP hub as well as the AOTU close to the loop in the SLP. It will be most promising to unravel these connections in further detail.

DATA AVAILABILITY STATEMENT

The raw data supporting the conclusions of this article will be made available by the authors, without undue reservation.

AUTHOR CONTRIBUTIONS

FS performed and analyzed experiments for the anatomy studies with the help of NH. NR performed and analyzed experiments for the anatomy and connectivity studies. EB, DR and GM acquired data for the connectivity studies, MS generated the DN_2 split-GAL4 line. NR analyzed the data, compiled the figures, and wrote the first version of the manuscript together with FS and CH-F. CH-F improved the manuscript and wrote the abstract and discussion with contributions from NR, EB, DR and TY. CH-F, DR and TY conceived the project, supervised the study, and contributed to funding.

FUNDING

This research was funded by the Deutsche Forschungsgemeinschaft (DFG, German Research Foundation) (grants FO 207/16-1, RI 2411/1-1 and for the Leica SP8: 251610680, INST 93/809-1 FUGG) and the JSPS KAKENHI (19H03265). Publication was supported by the Open Access Publication Fund of the University of Würzburg. We thank Heinrich Dirksen for ITP antisera, Ralf Stanewsky for PER antisera and Takeshi Todo for CRY antisera, Jan Veenstra for antibodies against AstC, and DH31 as well as Fumika Hamada for the *Clk9M-Gal4; pdf-Gal80* fly line, and Patrick Greguletz for help with preparing and immunostaining. Furthermore, we are grateful to Maria Fernandez and Orié Shafer for communicating results prior to publication.

SUPPLEMENTARY MATERIAL

The Supplementary Material for this article can be found online at: <https://www.frontiersin.org/articles/10.3389/fphys.2022.886432/full#supplementary-material>

Ahmad, M., Li, W., and Top, D. (2021). Integration of Circadian Clock Information in the Drosophila Circadian Neuronal Network. *J. Biol. Rhythms* 36, 203–220. doi:10.1177/0748730421993953

Alpert, M. H., Frank, D. D., Kaspi, E., Flourakis, M., Zaharieva, E. E., Allada, R., et al. (2020). A Circuit Encoding Absolute Cold Temperature in Drosophila. *Curr. Biol.* 30, 2275–2288. e5. doi:10.1016/j.cub.2020.04.038

- Arshadi, C., Günther, U., Eddison, M., Harrington, K. I. S., and Ferreira, T. A. (2021). SNT: a Unifying Toolbox for Quantification of Neuronal Anatomy. *Nat. Methods* 18, 374–377. doi:10.1038/s41592-021-01105-7
- Azevedo, R. V. D. M. d., Hansen, C., Chen, K.-F., Rosato, E., and Kyriacou, C. P. (2020). Disrupted Glutamate Signaling in *Drosophila* Generates Locomotor Rhythms in Constant Light. *Front. Physiol.* 11, 145. doi:10.3389/fphys.2020.00145
- Barber, A. F., Erion, R., Holmes, T. C., and Sehgal, A. (2016). Circadian and Feeding Cues Integrate to Drive Rhythms of Physiology in *Drosophila* Insulin-Producing Cells. *Genes Dev.* 30, 2596–2606. doi:10.1101/gad.288258.116
- Bates, A. S., and Jefferis, G. S. X. E. (2022). Hemibrain: Code for Working with Data from Janelia FlyEM's Hemibrain Project and the Flywire Data Sets. Available at: <https://github.com/flyconnectome/hemibrain>.
- Bates, A. S., Manton, J. D., Jagannathan, S. R., Costa, M., Schlegel, P., Rohlfing, T., et al. (2020). The Natverse, a Versatile Toolbox for Combining and Analysing Neuroanatomical Data. *eLife* 9, e53350. doi:10.7554/eLife.53350
- Beckwith, E. J., and Ceriani, M. F. (2015). Communication between Circadian Clusters: The Key to a Plastic Network. *FEBS Lett.* 589, 3336–3342. doi:10.1016/j.febslet.2015.08.017
- Benito, J., Houl, J. H., Roman, G. W., and Hardin, P. E. (2008). The Blue-Light Photoreceptor CRYPTOCHROME Is Expressed in a Subset of Circadian Oscillator Neurons in the *Drosophila* CNS. *J. Biol. Rhythms* 23, 296–307. doi:10.1177/0748730408318588
- Bertolini, E., and Helfrich-Förster, C. (2021). “Sleep and the Circadian Clock in Insects,” in *Reference Module in Neuroscience and Biobehavioral Psychology* (Amsterdam, Netherlands: Elsevier). doi:10.1016/B978-0-12-822963-7.00037-2
- Bogovic, J. A., Otsuna, H., Heinrich, L., Ito, M., Jeter, J., Meissner, G., et al. (2020). An Unbiased Template of the *Drosophila* Brain and Ventral Nerve Cord. *PLOS ONE* 15, e0236495. doi:10.1371/journal.pone.0236495
- Buhl, E., Bradlaugh, A., Ogueta, M., Chen, K.-F., Stanewsky, R., and Hodge, J. J. L. (2016). Quasimodo Mediates Daily and Acute Light Effects on *Drosophila* Clock Neuron Excitability. *Proc. Natl. Acad. Sci. U.S.A.* 113, 13486–13491. doi:10.1073/pnas.1606547113
- Cavanaugh, D. J., Geratowski, J. D., Wooltorton, J. R. A., Spaethling, J. M., Hector, C. E., Zheng, X., et al. (2014). Identification of a Circadian Output Circuit for Rest-activity Rhythms in *Drosophila*. *Cell* 157, 689–701. doi:10.1016/j.cell.2014.02.024
- Chatterjee, A., Lamaze, A., De, J., Mena, W., Chélot, E., Martin, B., et al. (2018). Reconfiguration of a Multi-Oscillator Network by Light in the *Drosophila* Circadian Clock. *Curr. Biol.* 28, 2007–2017. e4. doi:10.1016/j.cub.2018.04.064
- Chen, J., Reiher, W., Hermann-Luibl, C., Sellami, A., Cognigni, P., Kondo, S., et al. (2016). Allatostatin A Signalling in *Drosophila* Regulates Feeding and Sleep and Is Modulated by PDF. *Plos Genet.* 12, e1006346. doi:10.1371/journal.pgen.1006346
- Chen, K. F., Peschel, N., Zavodskaya, R., Sehadow, H., and Stanewsky, R. (2011). QUASIMODO, a Novel GPI-Anchored Zona Pellucida Protein Involved in Light Input to the *Drosophila* Circadian Clock. *Curr. Biol.* 21, 719–729. doi:10.1016/j.cub.2011.03.049
- Collins, B., Kane, E. A., Reeves, D. C., Akabas, M. H., and Blau, J. (2012). Balance of Activity between LNvs and Glutamatergic Dorsal Clock Neurons Promotes Robust Circadian Rhythms in *Drosophila*. *Neuron* 74, 706–718. doi:10.1016/j.neuron.2012.02.034
- Díaz, M. M., Schlichting, M., Abruzzi, K. C., Long, X., and Rosbash, M. (2019). Allatostatin-C/AstC-R2 Is a Novel Pathway to Modulate the Circadian Activity Pattern in *Drosophila*. *Curr. Biol.* 29, 13–22. e3. doi:10.1016/j.cub.2018.11.005
- Ewer, J., Frisch, B., Hamblen-Coyle, M., Rosbash, M., and Hall, J. (1992). Expression of the Period Clock Gene within Different Cell Types in the Brain of *Drosophila* Adults and Mosaic Analysis of These Cells' Influence on Circadian Behavioral Rhythms. *J. Neurosci.* 12, 3321–3349. doi:10.1523/JNEUROSCI.12-09-03321.1992
- Frenkel, L., Muraro, N. I., Beltrán González, A. N., Marcora, M. S., Bernabó, G., Hermann-Luibl, C., et al. (2017). Organization of Circadian Behavior Relies on Glycinergic Transmission. *Cel Rep.* 19, 72–85. doi:10.1016/j.celrep.2017.03.034
- Frisch, B., Hardin, P. E., Hamblen-Coyle, M. J., Rosbash, M., and Hall, J. C. (1994). A Promoterless Period Gene Mediates Behavioral Rhythmicity and Cyclical Per Expression in a Restricted Subset of the *Drosophila* Nervous System. *Neuron* 12, 555–570. doi:10.1016/0896-6273(94)90212-7
- Fujiwara, Y., Hermann-Luibl, C., Katsura, M., Sekiguchi, M., Ida, T., Helfrich-Förster, C., et al. (2018). The CCHamide1 Neuropeptide Expressed in the Anterior Dorsal Neuron 1 Conveys a Circadian Signal to the Ventral Lateral Neurons in *Drosophila melanogaster*. *Front. Physiol.* 9, 1276. doi:10.3389/fphys.2018.01276
- George, R., and Stanewsky, R. (2021). Peripheral Sensory Organs Contribute to Temperature Synchronization of the Circadian Clock in *Drosophila melanogaster*. *Front. Physiol.* 12. doi:10.3389/fphys.2021.622545
- Goda, T., Doi, M., Umezaki, Y., Murai, I., Shimatani, H., Chu, M. L., et al. (2018). Calcitonin Receptors Are Ancient Modulators for Rhythms of Preferential Temperature in Insects and Body Temperature in Mammals. *Genes Dev.* 32, 140–155. doi:10.1101/gad.307884.117
- Goda, T., Tang, X., Umezaki, Y., Chu, M. L., Kunst, M., Nitabach, M. N., et al. (2016). *Drosophila* DH31 Neuropeptide and PDF Receptor Regulate Night-Onset Temperature Preference. *J. Neurosci.* 36, 11739–11754. doi:10.1523/JNEUROSCI.0964-16.2016
- Goda, T., Umezaki, Y., Alwattari, F., Seo, H. W., and Hamada, F. N. (2019). Neuropeptides PDF and DH31 Hierarchically Regulate Free-Running Rhythmicity in *Drosophila* Circadian Locomotor Activity. *Sci. Rep.* 9. doi:10.1038/s41598-018-37107-3
- Grima, B., Chélot, E., Xia, R., and Rouyer, F. (2004). Morning and Evening Peaks of Activity Rely on Different Clock Neurons of the *Drosophila* Brain. *Nature* 431, 869–873. doi:10.1038/nature02935
- Gummadova, J. O., Coutts, G. A., and Glossop, N. R. J. (2009). Analysis of the *Drosophila* Clock Promoter Reveals Heterogeneity in Expression between Subgroups of Central Oscillator Cells and Identifies a Novel Enhancer Region. *J. Biol. Rhythms* 24, 353–367. doi:10.1177/0748730409343890
- Guo, F., Holla, M., Diaz, M. M., and Rosbash, M. (2018). A Circadian Output Circuit Controls Sleep-Wake Arousal in *Drosophila*. *Neuron* 100, 624–635. e4. doi:10.1016/j.neuron.2018.09.002
- Guo, F., Yu, J., Jung, H. J., Abruzzi, K. C., Luo, W., Griffith, L. C., et al. (2016). Circadian Neuron Feedback Controls the *Drosophila* Sleep-Activity Profile. *Nature* 536, 292–297. doi:10.1038/nature19097
- Hadjieconomou, D., Rotkopf, S., Alexandre, C., Bell, D. M., Dickson, B. J., and Salecker, I. (2011). Flybow: Genetic Multicolor Cell Labeling for Neural Circuit Analysis in *Drosophila melanogaster*. *Nat. Methods* 8, 260–266. doi:10.1038/nmeth.1567
- Hamada, F. N., Rosenzweig, M., Kang, K., Pulver, S. R., Ghezzi, A., Jegla, T. J., et al. (2008). An Internal Thermal Sensor Controlling Temperature Preference in *Drosophila*. *Nature* 454, 217–220. doi:10.1038/nature07001
- Hamasaka, Y., Rieger, D., Parmentier, M.-L., Grau, Y., Helfrich-Förster, C., and Nässel, D. R. (2007). Glutamate and its Metabotropic Receptor in *Drosophila* Clock Neuron Circuits. *J. Comp. Neurol.* 505, 32–45. doi:10.1002/cne.21471
- Harper, R. E. F., Dayan, P., Albert, J. T., and Stanewsky, R. (2016). Sensory Conflict Disrupts Activity of the *Drosophila* Circadian Network. *Cel Rep.* 17, 1711–1718. doi:10.1016/j.celrep.2016.10.029
- Helfrich-Förster, C. (2005). Neurobiology of the Fruit Fly's Circadian Clock. *Genes, Brain Behav.* 4, 65–76. doi:10.1111/j.1601-183X.2004.00092.x
- Helfrich-Förster, C., Shafer, O. T., Wülbeck, C., Grieshaber, E., Rieger, D., and Taghert, P. (2007a). Development and Morphology of the Clock-Gene-Expressing Lateral Neurons of *Drosophila melanogaster*. *J. Comp. Neurol.* 500, 47–70. doi:10.1002/cne.21146
- Helfrich-Förster, C., Stengl, M., and Homberg, U. (1998). Organization of the Circadian System in Insects. *Chronobiology Int.* 15, 567–594. doi:10.3109/07420529808993195
- Helfrich-Förster, C. (2017). “The *Drosophila* Clock System,” in *Biological Timekeeping: Clocks, Rhythms and Behaviour*. Editor V. Kumar (New Delhi: Springer India), 133–176. doi:10.1007/978-81-322-3688-7_6
- Helfrich-Förster, C. (2003). The Neuroarchitecture of the Circadian Clock in the Brain of *Drosophila melanogaster*. *Microsc. Res. Tech.* 62, 94–102. doi:10.1002/jemt.10357
- Helfrich-Förster, C., Yoshii, T., Wülbeck, C., Grieshaber, E., Rieger, D., Bachleitner, W., et al. (2007b). The Lateral and Dorsal Neurons of *Drosophila melanogaster*: New Insights about Their Morphology and Function. *Cold Spring Harbor Symposia Quantitative Biol.* 72, 517–525. doi:10.1101/sqb.2007.72.063
- Herzog, E. D., Hermanstyn, T., Smyllie, N. J., and Hastings, M. H. (2017). Regulating the Suprachiasmatic Nucleus (SCN) Circadian Clockwork: Interplay between Cell-Autonomous and Circuit-Level Mechanisms. *Cold Spring Harb Perspect. Biol.* 9, a027706. doi:10.1101/cshperspect.a027706

- Im, S. H., Li, W., and Taghert, P. H. (2011). PDFR and CRY Signaling Converge in a Subset of Clock Neurons to Modulate the Amplitude and Phase of Circadian Behavior in *Drosophila*. *PLoS ONE* 6, e18974. doi:10.1371/journal.pone.0018974
- Im, S. H., and Taghert, P. H. (2010). PDF Receptor Expression Reveals Direct Interactions between Circadian Oscillators in *Drosophila*. *J. Comp. Neurol.* 518, 1925–1945. doi:10.1002/cne.22311
- Jefferis, G. S. X. E., Potter, C. J., Chan, A. M., Marin, E. C., Rohlffing, T., Maurer, C. R., et al. (2007). Comprehensive Maps of *Drosophila* Higher Olfactory Centers: Spatially Segregated Fruit and Pheromone Representation. *Cell* 128, 1187–1203. doi:10.1016/j.cell.2007.01.040
- Jin, X., Tian, Y., Zhang, Z. C., Gu, P., Liu, C., and Han, J. (2021). A Subset of DN1p Neurons Integrates Thermosensory Inputs to Promote Wakefulness via CNMa Signaling. *Curr. Biol.* 31, 2075–2087. e6. doi:10.1016/j.cub.2021.02.048
- Jung, S.-H., Lee, J.-H., Chae, H.-S., Seong, J. Y., Park, Y., Park, Z.-Y., et al. (2014). Identification of a Novel Insect Neuropeptide, CNMa and its Receptor. *FEBS Lett.* 588, 2037–2041. doi:10.1016/j.febslet.2014.04.028
- Kaneko, H., Head, L. M., Ling, J., Tang, X., Liu, Y., Hardin, P. E., et al. (2012). Circadian Rhythm of Temperature Preference and its Neural Control in *Drosophila*. *Curr. Biol.* 22, 1851–1857. doi:10.1016/j.cub.2012.08.006
- Kaneko, M., Helfrich-Förster, C., and Hall, J. C. (1997). Spatial and Temporal Expression of the period and timeless Genes in the Developing Nervous System of *Drosophila*: Newly Identified Pacemaker Candidates and Novel Features of Clock Gene Product Cycling. *J. Neurosci.* 17, 6745–6760. doi:10.1523/JNEUROSCI.17-17-06745.1997
- Kind, E., Longden, K. D., Nern, A., Zhao, A., Sancer, G., Flynn, M. A., et al. (2021). Synaptic Targets of Photoreceptors Specialized to Detect Color and Skylight Polarization in *Drosophila*. *eLife* 10, e71858. doi:10.7554/eLife.71858
- King, A. N., and Sehgal, A. (2020). Molecular and Circuit Mechanisms Mediating Circadian Clock Output in the *Drosophila* Brain. *Eur. J. Neurosci.* 51, 268–281. doi:10.1111/ejn.14092
- Kunst, M., Hughes, M. E., Raccuglia, D., Felix, M., Li, M., Barnett, G., et al. (2014). Calcitonin Gene-Related Peptide Neurons Mediate Sleep-specific Circadian Output in *Drosophila*. *Curr. Biol.* 24, 2652–2664. doi:10.1016/j.cub.2014.09.077
- Lamaze, A., Krättschmer, P., Chen, K.-F., Lowe, S., and Jepson, J. E. C. (2018). A Wake-Promoting Circadian Output Circuit in *Drosophila*. *Curr. Biol.* 28, 3098–3105. e3. doi:10.1016/j.cub.2018.07.024
- Lamaze, A., and Stanewsky, R. (2020). DN1p or the “Fluffy” Cerberus of Clock Outputs. *Front. Physiol.* 10. doi:10.3389/fphys.2019.01540
- Li, J., Mahoney, B. D., Jacob, M. S., and Caron, S. J. C. (2020). Visual Input into the *Drosophila melanogaster* Mushroom Body. *Cel. Rep.* 32, 108138. doi:10.1016/j.celrep.2020.108138
- Li, M.-T., Cao, L.-H., Xiao, N., Tang, M., Deng, B., Yang, T., et al. (2018). Hub-organized Parallel Circuits of central Circadian Pacemaker Neurons for Visual Photoentrainment in *Drosophila*. *Nat. Commun.* 9, 4247. doi:10.1038/s41467-018-06506-5
- Lin, H.-H., Kuang, M. C., Hossain, I., Xuan, Y., Beebe, L., Shepherd, A. K., et al. (2022). A Nutrient-specific Gut Hormone Arbitrates between Courtship and Feeding. *Nature* 602, 632–638. doi:10.1038/s41586-022-04408-7
- Ma, D., Przybylski, D., Abruzzi, K. C., Schlichting, M., Li, Q., Long, X., et al. (2021). A Transcriptomic Taxonomy of *Drosophila* Circadian Neurons Around the Clock. *eLife* 10, e63056. doi:10.7554/eLife.63056
- Marin, E. C., Büld, L., Theiss, M., Sarkissian, T., Roberts, R. J. V., Turnbull, R., et al. (2020). Connectomics Analysis Reveals First-, Second-, and Third-Order Thermosensory and Hyposensory Neurons in the Adult *Drosophila* Brain. *Curr. Biol.* 30, 3167–3182. e4. doi:10.1016/j.cub.2020.06.028
- Meiselman, M. R., Alpert, M. H., Cui, X., Shea, J., Gregg, I., Gallio, M., et al. (2022). Recovery from Cold-Induced Reproductive Dormancy Is Regulated by Temperature-dependent AstC Signaling. *Curr. Biol.* 32, 1362–1375. doi:10.1016/j.cub.2022.01.061
- Michel, S., and Meijer, J. H. (2020). From Clock to Functional Pacemaker. *Eur. J. Neurosci.* 51, 482–493. doi:10.1111/ejn.14388
- Mieda, M. (2020). The central Circadian Clock of the Suprachiasmatic Nucleus as an Ensemble of Multiple Oscillatory Neurons. *Neurosci. Res.* 156, 24–31. doi:10.1016/j.neures.2019.08.003
- Miyasako, Y., Umezaki, Y., and Tomioka, K. (2007). Separate Sets of Cerebral Clock Neurons Are Responsible for Light and Temperature Entrainment of *Drosophila* Circadian Locomotor Rhythms. *J. Biol. Rhythms* 22, 115–126. doi:10.1177/0748730407299344
- Nagoshi, E., Sugino, K., Kula, E., Okazaki, E., Tachibana, T., Nelson, S., et al. (2010). Dissecting Differential Gene Expression within the Circadian Neuronal Circuit of *Drosophila*. *Nat. Neurosci.* 13, 60–68. doi:10.1038/nm.2451
- Ni, J. D., Gurav, A. S., Liu, W., Ogunmowo, T. H., Hackbart, H., Elsheikh, A., et al. (2019). Differential Regulation of the *Drosophila* Sleep Homeostat by Circadian and Arousal Inputs. *eLife* 8, e40487. doi:10.7554/eLife.40487
- Nicolai, L. J., Ramaekers, A., Ramaekers, T., Drozdzecki, A., Mauss, A. S., Yan, J., et al. (2010). Genetically Encoded Dendritic Marker Sheds Light on Neuronal Connectivity in *Drosophila*. *Proc. Natl. Acad. Sci. U.S.A.* 107, 20553–20558. doi:10.1073/pnas.1010198107
- Pfeiffer, B. D., Jenett, A., Hammonds, A. S., Ngo, T.-T. B., Misra, S., Murphy, C., et al. (2008). Tools for Neuroanatomy and Neurogenetics in *Drosophila*. *Proc. Natl. Acad. Sci. U.S.A.* 105, 9715–9720. doi:10.1073/pnas.0803697105
- Pfeiffer, B. D., Ngo, T.-T. B., Hibbard, K. L., Murphy, C., Jenett, A., Truman, J. W., et al. (2010). Refinement of Tools for Targeted Gene Expression in *Drosophila*. *Genetics* 186, 735–755. doi:10.1534/genetics.110.119917
- Picot, M., Klarsfeld, A., Chélot, E., Malpel, S., and Rouyer, F. (2009). A Role for Blind DN2 Clock Neurons in Temperature Entrainment of the *Drosophila* Larval Brain. *J. Neurosci.* 29, 8312–8320. doi:10.1523/JNEUROSCI.0279-08.2009
- Reinhard, N., Bertolini, E., Saito, A., Sekiguchi, M., Yoshii, T., Rieger, D., et al. (2022). The Lateral Posterior Clock Neurons of *Drosophila melanogaster* Express Three Neuropeptides and Have Multiple Connections within the Circadian Clock Network and beyond. *J. Comp. Neurol.* doi:10.1002/cne.25294
- Renn, S. C. P., Park, J. H., Rosbash, M., Hall, J. C., and Taghert, P. H. (1999). A Pdf Neuropeptide Gene Mutation and Ablation of PDF Neurons Each Cause Severe Abnormalities of Behavioral Circadian Rhythms in *Drosophila*. *Cell* 99, 791–802. doi:10.1016/S0092-8674(00)81676-1
- Rohlffing, T., and Maurer, C. R. (2003). Nonrigid Image Registration in Shared-Memory Multiprocessor Environments with Application to Brains, Breasts, and Bees. *IEEE Trans. Inform. Technol. Biomed.* 7, 16–25. doi:10.1109/TITB.2003.808506
- Rojas, P., Plath, J. A., Gestrich, J., Ananthasubramaniam, B., Garcia, M. E., Herzog, H., et al. (2019). Beyond Spikes: Multiscale Computational Analysis of In Vivo Long-Term Recordings in the Cockroach Circadian Clock. *Netw. Neurosci.* 3, 944–968. doi:10.1162/netn_a_00106
- Scheffer, L. K., Xu, C. S., Januszewski, M., Lu, Z., Takemura, S. Y., Hayworth, K. J., et al. (2020). A Connectome and Analysis of the Adult *Drosophila* central Brain. *eLife* 9, e57443. doi:10.7554/eLife.57443
- Schindelin, J., Arganda-Carreras, I., Frise, E., Kaynig, V., Longair, M., Pietzsch, T., et al. (2012). Fiji: an Open-Source Platform for Biological-Image Analysis. *Nat. Methods* 9, 676–682. doi:10.1038/nmeth.2019
- Schubert, F. K., Hagedorn, N., Yoshii, T., Helfrich-Förster, C., and Rieger, D. (2018). Neuroanatomical Details of the Lateral Neurons of *Drosophila melanogaster* support Their Functional Role in the Circadian System. *J. Comp. Neurol.* 526, 1209–1231. doi:10.1002/cne.24406
- Shadova, H., Glaser, F. T., Gentile, C., Simoni, A., Giesecke, A., Albert, J. T., et al. (2009). Temperature Entrainment of *Drosophila*'s Circadian Clock Involves the Gene *Nocte* and Signaling from Peripheral Sensory Tissues to the Brain. *Neuron* 64, 251–266. doi:10.1016/j.neuron.2009.08.026
- Sekiguchi, M., Inoue, K., Yang, T., Luo, D.-G., and Yoshii, T. (2020). A Catalog of GAL4 Drivers for Labeling and Manipulating Circadian Clock Neurons in *Drosophila melanogaster*. *J. Biol. Rhythms* 35, 207–213. doi:10.1177/0748730419895154
- Shafer, O. T., Helfrich-Förster, C., Renn, S. C. P., and Taghert, P. H. (2006). Reevaluation of *Drosophila melanogaster*'s Neuronal Circadian Pacemakers Reveals New Neuronal Classes. *J. Comp. Neurol.* 498, 180–193. doi:10.1002/cne.21021
- Shafer, O. T., Kim, D. J., Dunbar-Yaffe, R., Nikolaev, V. O., Lohse, M. J., and Taghert, P. H. (2008). Widespread Receptivity to Neuropeptide PDF throughout the Neuronal Circadian Clock Network of *Drosophila* Revealed by Real-Time Cyclic AMP Imaging. *Neuron* 58, 223–237. doi:10.1016/j.neuron.2008.02.018
- Shimosaki, N., Hadjieconomou, D., and Salecker, I. (2014). Flybow to Dissect Circadian Assembly in the *Drosophila* Brain. *Methods Mol. Biol.* 1082, 57–69. doi:10.1007/978-1-62703-655-9_4

- Song, B. J., Sharp, S. J., and Rogulja, D. (2021). Daily Rewiring of a Neural Circuit Generates a Predictive Model of Environmental Light. *Sci. Adv.* 7, eabe4284. doi:10.1126/sciadv.abe4284
- Stengl, M., and Arendt, A. (2016). Peptidergic Circadian Clock Circuits in the Madeira Cockroach. *Curr. Opin. Neurobiol.* 41, 44–52. doi:10.1016/j.conb.2016.07.010
- Talay, M., Richman, E. B., Snell, N. J., Hartmann, G. G., Fisher, J. D., Sorkaç, A., et al. (2017). Transsynaptic Mapping of Second-Order Taste Neurons in Flies by Trans-tango. *Neuron* 96, 783–795. e4. doi:10.1016/j.neuron.2017.10.011
- Tang, X., Roessingh, S., Hayley, S. E., Chu, M. L., Tanaka, N. K., Wolfgang, W., et al. (2017). The Role of PDF Neurons in Setting the Preferred Temperature before Dawn in *Drosophila*. *eLife* 6, e23206. doi:10.7554/eLife.23206
- Top, D., and Young, M. W. (2018). Coordination between Differentially Regulated Circadian Clocks Generates Rhythmic Behavior. *Cold Spring Harb Perspect. Biol.* 10, a033589. doi:10.1101/cshperspect.a033589
- Wickham, H. (2016). *ggplot2: Elegant Graphics for Data Analysis*. 2nd ed. Berlin, Germany: Springer International Publishing. doi:10.1007/978-3-319-24277-4
- Yadlapalli, S., Jiang, C., Bahle, A., Reddy, P., Meyhofer, E., and Shafer, O. T. (2018). Circadian Clock Neurons Constantly Monitor Environmental Temperature to Set Sleep Timing. *Nature* 555, 98–102. doi:10.1038/nature25740
- Yoshii, T., Todo, T., Wülbeck, C., Stanewsky, R., and Helfrich-Förster, C. (2008). Cryptochrome Is Present in the Compound Eyes and a Subset of *Drosophila*'s Clock Neurons. *J. Comp. Neurol.* 508, 952–966. doi:10.1002/cne.21702
- Yoshii, T., Vanin, S., Costa, R., and Helfrich-Förster, C. (2009). Synergic Entrainment of *Drosophila*'s Circadian Clock by Light and Temperature. *J. Biol. Rhythms* 24, 452–464. doi:10.1177/0748730409348551
- Zerr, D., Hall, J., Rosbash, M., and Siwicki, K. (1990). Circadian Fluctuations of Period Protein Immunoreactivity in the CNS and the Visual System of *Drosophila*. *J. Neurosci.* 10, 2749–2762. doi:10.1016/j.cub.2013.02.05710.1523/jneurosci.10-08-02749.1990
- Zhang, C., Dauberova, I., Jang, Y.-H., Kondo, S., Žitňan, D., and Kim, Y.-J. (2021). The Neuropeptide Allatostatin C from Clock-Associated DN1p Neurons Generates the Circadian Rhythm for Oogenesis. *Proc. Natl. Acad. Sci. U.S.A.* 118, e2016878118. doi:10.1073/pnas.2016878118
- Zhang, L., Chung, B. Y., Lear, B. C., Kilman, V. L., Liu, Y., Mahesh, G., et al. (2010a). DN1p Circadian Neurons Coordinate Acute Light and PDF Inputs to Produce Robust Daily Behavior in *Drosophila*. *Curr. Biol.* 20, 591–599. doi:10.1016/j.cub.2010.02.056
- Zhang, Y., Liu, Y., Bilodeau-Wentworth, D., Hardin, P. E., and Emery, P. (2010b). Light and Temperature Control the Contribution of Specific DN1 Neurons to *Drosophila* Circadian Behavior. *Curr. Biol.* 20, 600–605. doi:10.1016/j.cub.2010.02.044
- Zhang, Y. Q., Rodesch, C. K., and Broadie, K. (2002). Living Synaptic Vesicle Marker: Synaptotagmin-GFP. *Genesis* 34, 142–145. doi:10.1002/gene.10144
- Zheng, Z., Lauritzen, J. S., Perlman, E., Robinson, C. G., Nichols, M., Milkie, D., et al. (2018). A Complete Electron Microscopy Volume of the Brain of Adult *Drosophila melanogaster*. *Cell* 174, 730–743. e22. doi:10.1016/j.cell.2018.06.019
- Conflict of Interest:** The authors declare that the research was conducted in the absence of any commercial or financial relationships that could be construed as a potential conflict of interest.
- Publisher's Note:** All claims expressed in this article are solely those of the authors and do not necessarily represent those of their affiliated organizations, or those of the publisher, the editors and the reviewers. Any product that may be evaluated in this article, or claim that may be made by its manufacturer, is not guaranteed or endorsed by the publisher.

Copyright © 2022 Reinhard, Schubert, Bertolini, Hagedorn, Manoli, Sekiguchi, Yoshii, Rieger and Helfrich-Förster. This is an open-access article distributed under the terms of the Creative Commons Attribution License (CC BY). The use, distribution or reproduction in other forums is permitted, provided the original author(s) and the copyright owner(s) are credited and that the original publication in this journal is cited, in accordance with accepted academic practice. No use, distribution or reproduction is permitted which does not comply with these terms.

GLOSSARY

AME accessory medulla	LD light-dark
AOTU anterior optic tubercle	I-DN₃ large dorsal neurons 3
AstC Allatostatin C	LH lateral horn
CA mushroom body calyx	I-LN_v large ventrolateral neurons
contr. contralateral	5th LN 5 th lateral neuron
CRY Cryptochrome	LN lateral neurons
DenMark dendritic marker	LN_d dorsolateral neurons
dFB dorsal fan-shaped body	LO lobula
DH31 diuretic hormone 31	LPN lateral posterior neurons
DN dorsal neurons	MDC middle dorsal commissure
DN_{1a} anterior dorsal neurons group 1	ME medulla
DN_{1p} posterior dorsal neurons group 1	myrGFP myristoylated GFP
DN_{1p-A} posterior remaining subtype of DN _{1p} (hemibrain nomenclature), also known as vc-DN _{1p} ()	nSyb neuronal Synaptobrevin
DN_{1p-B} anterior projecting subtype of DN _{1p} (hemibrain nomenclature), also known as a-DN _{1p} ()	OL optic lobe
DN₂ dorsal neurons group 2	PDF Pigment dispersing factor
DN₃ dorsal neurons group 3	PDFR PDF receptor
EGFP enhanced green fluorescent protein	PER Period
FAFB full adult female brain (electron microscopic dataset)	PI pars intercerebralis
FB fan-shaped body of the central complex	PL pars lateralis
FB2.0B <i>UAS-Flybow2.0B</i> ; refers to the Flybow system	PLP posterior lateral protocerebrum
GFP green fluorescent protein	SAC superior arch commissure
HA hemagglutinin	SCL superior clamp
hs-Flp heat shock FLP recombinase	s-DN₃ small dorsal neurons 3
ICL inferior clamp	SEZ subesophageal zone
ipsi. ipsilateral	s-LN_v small ventrolateral neurons
ITP ion transport peptide	SLP superior lateral protocerebrum
	SMP superior medial protocerebrum
	UAS upstream activating sequence
	ZT Zeitgeber time